THE ASTRONOMICAL JOURNAL, 115:1745–1777, 1998 May

THE STAR FORMATION PROPERTIES OF DISK GALAXIES: Hα IMAGING OF GALAXIES IN THE COMA SUPERCLUSTER[1]

GIUSEPPE GAVAZZI[2] AND BARBARA CATINELLA
Dipartimento di Fisica, Università degli Studi di Milano, via Celoria 16, I-20133 Milano, Italy; gavazzi@brera.mi.astro.it, catinel@trane.uni.mi.astro.it

LUIS CARRASCO[3]
Instituto Nacional de Astrofísica, Optica y Electrónica, Apdo. Postal 51 y 216, 72000 Puebla, Pue., Mexico; carrasco@inaoep.mx

ALESSANDRO BOSELLI
Laboratoire d'Astronomie Spatiale, Traverse du Syphon, B.P. 8, F-13376 Marseille, France; boselli@astrsp-mrs.fr

AND

ALESSANDRA CONTURSI
Département de Radioastronomie Millimétrique, Observatoire de Paris, 61 Avenue de l'Observatoire, F-75014 Paris, France; contursi@mesioq.obspm.fr

Received 1997 June 25; revised 1997 November 4

ABSTRACT

We present integrated Hα measurements obtained from imaging observations of 98 late-type galaxies, primarily selected in the Coma supercluster. These data, combined with Hα photometry from the literature, include a magnitude-selected sample of spiral (Sa to Irr) galaxies belonging to the "Great Wall" complete up to $m_p = 15.4$, and thus composed of galaxies brighter than $M_p = -18.8$ ($H_0 = 100$ km s^{-1} Mpc^{-1}). The frequency distribution of the Hα equivalent width, determined for the first time from an optically complete sample, is approximately Gaussian, peaking at EW ~ 25 Å. We find that, at the present limiting luminosity, the star formation properties of spiral + Irr galaxy members of the Coma and A1367 Clusters do not differ significantly from those of the isolated ones belonging to the Great Wall. The present analysis confirms the well-known increase of the current massive star formation rate (SFR) with Hubble type. Moreover, perhaps a more fundamental anticorrelation exists between the SFR and the mass of disk galaxies: low-mass spirals and dwarf systems have present SFRs ~ 50 times higher than giant spirals. This result is consistent with the idea that disk galaxies are coeval, evolving as "closed systems" with exponentially declining SFR, and that the mass of their progenitor protogalaxies is the principal parameter governing their evolution. Massive systems having high initial efficiency of collapse, or a short collapse timescale, have retained little gas to feed the present epoch of star formation. These findings support the conclusions of Gavazzi & Scodeggio, who studied the color-mass relation of a local galaxy sample, and agree with the analysis by Cowie et al., who traced the star formation history of galaxies up to $z > 1$.

Key words: galaxies: evolution — galaxies: formation

1. INTRODUCTION

Two major aspects of the phenomenology of disk galaxies, with relevant implications for the theory of galaxy formation and evolution, are still hotly debated among the scientific community: (1) whether the color-luminosity relation, well established among late-type galaxies, follows from a population sequence, as proposed by Gavazzi, Pierini, & Boselli (1996, hereafter GPB96) and by Gavazzi & Scodeggio (1996, hereafter GS96), as opposed to a metallicity sequence (see Visvanathan 1991; Bothun et al. 1984), which appears to be the case in elliptical galaxies (see Arimoto & Kodama 1997); (2) whether the current star formation rate (SFR) of spiral galaxies belonging to a rich cluster is significantly lower than that of isolated galaxies of similar morphological type, as expected if either formation or evolutionary processes (e.g., ram pressure) contributed to the depletion of the gaseous content of spiral galaxies in clusters, thus reducing the gas reservoir necessary to feed their star formation.

Kennicutt's pioneering work in this field helped to establish that the massive ($>10\ M_\odot$), current ($t < 10^7$ yr) star formation rate of disk galaxies is accurately traced by the integrated Hα + [N II] line intensity (Kennicutt 1983a) normalized to the underlying continuum intensity (Kennicutt 1989, 1990), i.e., by the line equivalent width (EW). More recently Kennicutt, Tamblyn, & Congdon (1994, hereafter KTC94) determined that the ratio of the present to the past rate increases from 0.01 to 1 along the Hubble sequence (from Sa to Irr), reflecting a change in the star formation properties of disks, and only secondarily a change in the bulge-to-disk ratio.

To investigate hypothesis 1, in § 5.1 of this paper we study the dependence of the Hα EW on near-infrared *H*-band luminosity. Our large (although not complete) sample of galaxies spans a broad range of luminosities for which Hα EW and *H*-band photometry are available. Following GPB96, we assume that the *H*-band luminosity is proportional to the galaxy dynamical mass.

To discuss point 2, we compare the systematic (i.e., derived from a survey having the character of completeness) Hα properties of spiral galaxies as a function of some indi-

[1] Based on observations made at the Observatorio Astronómico Nacional (OAN), San Pedro Mártir, B.C., of the Universidad Nacional Autónoma de México (UNAM).

[2] Also Osservatorio Astronomico di Brera, via Brera 28, I-20121, Milano, Italy.

[3] Also OAN/UNAM, Ensenada, B.C., Mexico.

cator of their environmental conditions, e.g., their local galaxy density or the projected radial distance from the cluster centers. To this purpose, Kennicutt & Kent (1983, hereafter KK83) carried out an Hα survey of galaxies belonging to the Virgo Cluster and compared them with isolated objects. Kennicutt (1983b) tentatively concluded that galaxies belonging to the core of this cluster have an SFR significantly quenched in comparison with normal galaxies. Kennicutt, Bothun, & Schommer (1984, hereafter KBS84) extended this study to other dynamical entities, such as the Cancer Cluster, Coma, and A1367. The sample they collected, however, was not sufficient to derive general conclusions. Neither sufficiently complete was the Hα study by Gavazzi, Boselli, & Kennicutt (1991, hereafter GBK91), who carried out an aperture photometry, narrowband survey of another 55 late-type galaxies in the Coma ridge. They found that a significant number of spiral + Irr galaxies projected onto the two clusters have surprisingly strong Hα emission. These include the blue galaxies found in the Coma Cluster by Bothun & Dressler (1986).

A problem affecting these early studies was the lack of a well-defined zero point for their environmental comparison, i.e., the properties of isolated galaxies were not known with sufficient accuracy. With the aim of establishing the present high-mass SFR of spiral galaxies in the universe and of comparing these properties in environments that differ by an order of magnitude in local galaxy density, we undertook the present Hα imaging survey. The Coma supercluster offers a unique test bed for such systematic study since it contains a filament of galaxies at constant distance from us (the "Great Wall"), and thus a volume-limited sample can be extracted from a magnitude-limited sample. Moreover, the properties of galaxies in two rich clusters such as Coma and A1367 (with a density of about three galaxies Mpc^{-3} brighter than 15.7) can be compared with those of relatively isolated galaxies (environments with about 10% of the cluster density) lying in the bridge between the two clusters at a similar distance from us, and thus suffering from similar distance biases.

2. SAMPLE

Imaging in the light of the Hα + [N II] line of galaxies selected primarily in the region of the Coma supercluster is reported in this work. Out of the 262 spiral galaxies brighter than $m_p = 15.7$ belonging to the "Great Wall" listed in the catalog of Gavazzi & Boselli (1996), we observed 90 objects. (Eight additional early-type galaxies were observed serendipitously in the target fields. These will be not used in the following analysis.) By themselves these objects do not constitute a complete sample. However, from the observations presented in this paper, in conjunction with Hα aperture photometry measurements taken from the literature (KK83; KBS84; Moss, Whittle, & Irwin 1988; Romanishin 1990; GBK91), two complete subsamples can be extracted:

The "cluster" sample contains 40 spiral galaxies (28 imaged in this work plus 12 from the literature) with $m_p \leq 15.4$, belonging to either A1367 or to the Coma Cluster (A1656);

The "isolated" sample contains 66 galaxies (44 imaged in this work plus 22 from the literature) with $m_p \leq 15.4$ in the "Great Wall" defined as isolated, i.e., whose nearest companion lies at a projected distance of more than 300 kpc.

These two samples are used in the present investigation to derive frequency distributions, which need to be extracted from a magnitude-complete sample (§§ 5.3–5.4). The remaining objects observed in this work and/or found in the literature will be used only in those analyses that do not depend upon completeness (§§ 5.1, 5.2). We remark that, since the studied galaxies belong to a structure (the Coma supercluster) approximately at constant distance from the observer, a volume-limited sample can be easily extracted from the present magnitude-complete sample.

Table 1 lists the observed galaxies as follows:

Column (*1*).—CGCG designation (Zwicky et al. 1961–1968).

Columns (*2*), (*3*).—NGC/IC and UGC (Nilson 1973) names.

Columns (*4*), (*5*).—B1950.0 celestial coordinates (1″–2″ uncertainty).

Columns (*6*), (*7*).—Major and minor axes as determined at the 25 mag arcsec^{-2} isophote (see Gavazzi & Boselli 1996).

Column (*8*).—Heliocentric velocity from the literature.

Column (*9*).—Cluster membership (see Gavazzi & Boselli 1996 for more details). Members of Coma and A1367 are those objects with a projected angular separation within 2° and 1°, respectively, from their X-ray centers. One galaxy belongs to the NGC 4794 Group, another to the NGC 3937 Group, in the foreground of the Coma supercluster. Two objects constitute a pair of galaxies in the Coma supercluster. Six filler galaxies belong to the Cancer Cluster, two are in the foreground of the Hercules supercluster, and one is a member of A2197. The remaining galaxies are isolated supercluster objects. We assume a distance of 65 Mpc for A1367, and 69 Mpc for Coma. Isolated supercluster objects are assumed to be at their redshift distance, using $H_0 = 100$ $\mathrm{km\ s^{-1}\ Mpc^{-1}}$.

Column (*10*).—The cluster membership according to the less restrictive criterion of Gavazzi, Randone, & Branchini (1995b). A galaxy is considered a cluster member if it lies within the "caustic" associated with the cluster's potential well.

Column (*11*).—Projected radial distance from the nearest cluster center.

Column (*12*).—Morphological type (see Gavazzi & Boselli 1996). The classification was performed on the best photographic material available: (*a*) the present frames; (*b*) broadband CCD frames; (*c*) KPNO 4 m plates (for the two clusters); and (*d*) Palomar Sky Survey (PSS) plates. The majority of galaxies in our sample have small angular sizes (1′–2′), and thus the classification error is probably up to two bins of Hubble type. In particular, the overabundance of Pec and Irr objects reflects our classification inability. Given the distance of the Coma supercluster, no Magellanic Irr type is included in this work. We classify as Irr any galaxy with no evident spiral structure or circular symmetry. We prefer to classify as Pec the otherwise normal objects with superposed peculiar features, such as bright spots and extra arms. Pec/c stands for peculiar/compact, Pec/ms for peculiar/multiple system.

Column (*13*).—Photographic magnitude from Zwicky et al. (1961–1968).

Columns (*14*), (*15*).—B_0^T and H_0^T magnitudes, corrected for internal extinction (see Gavazzi & Boselli 1996).

The sky distribution of CGCG galaxies that are members of the Coma supercluster, and thus restricted to the velocity range 5000–10,000 $\mathrm{km\ s^{-1}}$, is shown in Figure 1.

TABLE 1

PARAMETERS OF THE TARGET GALAXIES

CGCG (1)	NGC (2)	UGC (3)	R.A. (B1950.0) (4)	DECL. (B1950.0) (5)	a (arcmin) (6)	b (arcmin) (7)	V_{hel} (km s^{-1}) (8)	MEMBERSHIP		θ (deg) (11)	TYPE (12)	m_p (mag) (13)	B_0^T (mag) (14)	H_0^T (mag) (15)
								Ang. Sep. (9)	Caustics (10)					
119035	...	...	08 15 00.20	22 35 32.0	1.35	0.38	2096	Cancer	Cancer	1.50	Sbc	15.40	14.57	12.23
119055	...	4332	08 16 43.00	21 16 20.0	2.97	0.50	5482	Cancer	Cancer	0.23	Pec	15.50	13.02	10.22
119078	...	4375	08 20 14.82	22 49 35.9	2.41	1.67	2061	Cancer	Cancer	1.71	Sc	14.60	12.98	9.86
119093	...	4400	08 23 10.30	21 49 56.0	1.25	0.25	4392	Cancer	Cancer	1.41	Sc	15.70	15.18	13.11
119096	...	4404	08 23 33.08	22 25 34.4	1.28	0.34	8491	Cancer	Cancer	1.81	Sc	15.50	14.21	11.87
119109	2595	4422	08 24 47.00	21 38 44.0	3.33	1.96	4332	Cancer	Cancer	1.70	Sc	13.90	12.25	9.33
127005	...	...	11 34 53.93	22 40 36.8	0.98	0.59	6864	Isolated	Isolated	3.04	Sbc	15.40	15.07	12.14
97062	...	...	11 39 38.88	20 15 11.3	1.01	0.40	7809	A1367	A1367	0.53	Pec	15.50	14.71	12.65
127033	...	6674	11 40 03.19	25 06 00.2	1.30	0.67	6300	Isolated	Isolated	5.02	Sc	15.20	14.32	11.41
97073	...	...	11 40 20.75	20 14 38.1	0.76	0.74	7290	A1367	A1367	0.37	Irr	15.60	15.71	13.28
127035	...	6681	11 40 25.79	24 13 19.0	1.20	0.30	6817	Isolated	Isolated	4.13	Sa	15.40	14.45	11.02
97079	...	...	11 40 37.69	20 16 55.6	0.75	0.45	6996	A1367	A1367	0.33	Irr	15.70	15.41	13.40
97078	...	6683	11 40 40.62	20 01 34.8	1.88	0.92	7526	A1367	A1367	0.27	Sa	15.20	13.81	11.16
97082	2951	6688	11 40 48.93	20 01 38.3	1.30	0.64	6100	A1367	A1367	0.24	Sa	15.00	14.57	10.25
127037	...	...	11 40 49.31	25 16 57.4	0.80	0.45	6186	Isolated	Isolated	5.19	Irr	15.40	14.76	12.77
97087	...	6697	11 41 13.19	20 14 49.1	2.00	0.50	6735	A1367	A1367	0.20	Irr	14.30	12.90	10.72
97092	...	...	11 41 22.52	20 27 46.3	0.76	0.54	6373	A1367	A1367	0.38	Sbc	15.50	15.35	12.61
97088	...	...	11 41 23.99	20 03 23.2	0.82	0.40	5552	A1367	A1367	0.10	S0	15.20	15.54	11.76
97093	...	...	11 41 26.30	20 03 42.9	0.96	0.39	4857	A1367	A1367	0.09	Pec	15.50	15.10	13.02
97102 S	...	...	11 41 40.80	20 29 40.4	0.93	0.27	...	A1367	A1367	0.40	E	15.50	15.39	11.27
97102 N	...	...	11 41 41.50	20 30 02.1	1.08	0.65	6361	A1367	A1367	0.40	Sa	15.10	14.75	11.03
97114	...	...	11 42 12.24	20 03 02.8	0.54	0.49	8522	A1367	A1367	0.11	Pec/c	15.40	15.89	13.19
97125	...	...	11 42 19.37	20 03 14.9	0.84	0.59	8288	A1367	A1367	0.13	S0a	15.60	15.55	11.82
97124	...	...	11 42 21.52	20 00 33.7	0.20	0.20	7809	A1367	A1367	0.16	E	15.30	...	12.26
97129 W	3861	6724	11 42 28.43	20 15 02.7	2.36	1.27	5082	A1367	A1367	0.22	Sb	14.00	13.24	9.87
97129 E	...	...	11 42 31.50	20 14 43.5	1.07	0.40	6009	A1367	A1367	0.22	Sbc	15.70	...	11.98
97138	...	...	11 43 09.38	20 18 31.1	0.75	0.64	5317	A1367	A1367	0.38	Irr	15.50	15.38	13.41
127052	3884	6746	11 43 36.73	20 40 10.8	1.70	1.26	6968	A1367	A1367	0.71	Sa	14.00	13.48	9.71
127053	...	6751	11 44 06.71	24 14 28.4	1.40	0.50	6409	Isolated	Isolated	4.18	Sbc	15.40	14.11	11.95
127054	3883	6754	11 44 11.78	20 57 10.7	3.10	2.80	7026	NGC 3937	A1367	1.02	Sb	14.20	13.52	10.31
157032	...	6761	11 44 31.56	29 51 20.1	1.53	0.55	6811	Isolated	Isolated	9.78	Sa	15.20	14.26	10.68
157044	...	...	11 48 48.00	27 03 45.0	0.70	0.30	6610	Isolated	Isolated	7.14	Pec	15.40	15.02	12.94
157064	3984	6943	11 55 17.50	29 19 03.6	1.41	0.95	6407	Isolated	Isolated	9.71	Sbc	14.80	14.22	11.60
98013	...	...	11 56 02.25	19 08 27.5	0.89	0.49	6949	Isolated	Isolated	3.49	Sc	15.10	14.48	11.75
98016	...	6986	11 56 53.25	18 02 03.2	1.38	0.43	6449	Isolated	A1367	4.12	Sc	15.30	14.04	11.88
98023	...	...	11 59 10.69	18 10 36.1	0.60	0.40	7075	Isolated	Isolated	4.53	Sb	15.10	15.14	11.76

TABLE 1—*Continued*

CGCG (1)	NGC (2)	UGC (3)	R.A. (B1950.0) (4)	Decl. (B1950.0) (5)	a (arcmin) (6)	b (arcmin) (7)	V_{hel} (km s^{-1}) (8)	Membership		θ (deg) (11)	Type (12)	m_p (mag) (13)	B_0^T (mag) (14)	H_0^T (mag) (15)
								Ang. Sep. (9)	Caustics (10)					
128015	...	...	12 02 22.87	21 31 09.7	0.70	0.60	6832	Isolated	Isolated	5.01	Sb	15.30	15.49	12.15
128021	...	7080	12 03 01.92	25 22 28.8	1.20	0.20	7064	Isolated	Isolated	7.19	Sbc	15.40	13.86	10.70
98058	4110	7102	12 04 30.25	18 48 34.8	1.36	0.73	7207	Isolated	Isolated	5.50	Sbc	14.70	14.15	10.63
158036	4146	7163	12 07 45.81	26 42 31.6	1.22	1.19	6532	Isolated	Isolated	8.89	Sb	13.80	14.04	10.34
98078	...	...	12 08 05.19	18 08 54.5	0.40	0.30	6838	Pair	Pair	6.51	E	15.20	...	12.35
98081	...	...	12 08 09.37	18 09 55.8	0.70	0.70	7191	Pair	Pair	6.52	Sa	15.20	15.24	11.61
98087	...	...	12 08 49.31	19 22 00.4	1.00	0.40	7527	Isolated	Isolated	6.40	...	15.30	14.83	11.36
98116	...	7263	12 12 53.00	19 34 11.4	1.04	0.79	6229	Isolated	Isolated	7.33	Sc	14.90	14.51	11.87
128066	IC 3075	...	12 13 23.12	23 52 23.9	0.90	0.50	6526	Isolated	Isolated	8.23	...	15.10	14.80	11.14
128072	...	...	12 15 36.82	24 57 58.1	0.50	0.50	6886	Isolated	Isolated	9.20	Pec	15.40	15.42	12.48
128073	IC 3122	7341	12 15 50.19	25 29 40.8	1.53	0.77	6949	Isolated	Isolated	9.52	Sb	14.70	13.99	11.15
158094	...	...	12 20 08.87	29 42 54.6	0.80	0.55	7951	Isolated	Isolated	8.30	...	15.30	15.24	12.09
128087	IC 3300	7495	12 22 34.31	26 14 05.7	1.10	0.28	6671	Isolated	Isolated	8.02	Sc	15.30	14.05	11.29
158105	IC 3330	7527	12 23 26.94	31 07 12.7	1.20	0.57	6824	Isolated	Isolated	7.93	Sbc	15.10	14.34	11.34
128089	IC 791	7555	12 24 28.81	22 54 57.5	1.10	1.10	6841	Isolated	Isolated	9.15	Sa	14.20	14.53	10.74
159008	4475	7632	12 27 18.00	27 31 10.4	1.70	1.02	7388	Isolated	Isolated	6.71	Sb	14.60	14.08	11.00
129004	...	...	12 27 19.12	22 38 53.9	0.70	0.50	6954	Isolated	Isolated	8.82	...	15.20	15.11	11.96
159033	IC 3598	7791	12 34 52.94	28 28 58.8	1.52	0.49	7673	Isolated	Isolated	4.98	Sa	15.00	14.30	10.75
99104	...	7815	12 36 31.56	18 28 30.8	1.28	0.42	7936	Isolated	Isolated	10.89	Sc	15.40	14.48	12.14
129020	IC 3692	7885	12 40 25.25	21 15 45.9	1.03	0.62	6579	Isolated	Isolated	7.99	Sb	14.80	14.51	10.87
159059	...	7890	12 40 38.31	27 59 16.7	0.85	0.62	7528	Isolated	Isolated	3.73	Sab	14.50	14.58	12.30
159061	...	...	12 40 47.69	31 21 33.2	1.09	1.02	6966	Isolated	A1656	4.77	Sbc	14.80	14.96	11.31
159095	IC 826	...	12 48 55.00	31 19 50.3	0.77	0.58	6837	Isolated	A1656	3.60	Sbc	14.90	15.02	11.26
100012	...	...	12 49 01.12	18 20 13.2	0.50	0.49	6481	Isolated	Isolated	10.10	Pec	15.30	15.55	12.71
159096	...	8004	12 49 13.25	31 37 28.7	1.67	0.62	6187	Isolated	Isolated	3.82	Sc	15.10	14.08	11.85
159097	...	...	12 49 40.60	27 17 52.0	0.56	0.46	6477	A1656	A1656	1.98	Pec	15.40	15.47	12.33
159101	...	...	12 50 22.90	27 40 25.0	0.55	0.46	7745	A1656	A1656	1.67	Pec	15.30	15.67	13.28
159102	...	8017	12 50 27.95	28 38 35.2	1.28	0.51	7057	A1656	A1656	1.60	Sab	14.50	13.84	10.45
160005	...	8025	12 51 37.50	29 52 26.0	1.87	0.43	6316	Isolated	A1656	2.07	Sb	14.80	13.86	10.22
160007	4788	...	12 51 50.20	27 34 27.0	1.02	0.40	6462	A1656	A1656	1.42	...	15.40	14.79	11.20
160018	...	...	12 53 02.30	27 55 35.0	0.87	0.44	7092	A1656	A1656	1.04	...	15.30	14.99	11.26
160020	...	...	12 53 40.69	27 56 53.6	0.66	0.32	4968	A1656?	Isolated	0.90	Pec/c	15.50	15.00	12.98
160025	4819	8060	12 54 02.81	27 15 30.0	1.19	0.86	6702	A1656	A1656	1.25	Sa	14.00	13.99	10.32
160026	IC 3913	...	12 54 03.12	27 33 42.5	0.85	0.55	7545	A1656	A1656	1.03	Sc	15.50	15.42	12.54
160024	4821	...	12 54 03.40	27 13 37.0	0.77	0.51	6980	A1656	A1656	1.28	E	15.00	15.06	11.35

TABLE 1—*Continued*

CGCG (1)	NGC (2)	UGC (3)	R.A. (B1950.0) (4)	Decl. (B1950.0) (5)	a (arcmin) (6)	b (arcmin) (7)	V_{hel} (km s^{-1}) (8)	Membership		θ (deg) (11)	Type (12)	m_p (mag) (13)	B_0^T (mag) (14)	H_0^T (mag) (15)
								Ang. Sep. (9)	Caustics (10)					
160032.....	IC 835	...	12 54 26.75	26 45 26.1	0.87	0.83	7747	A1656	A1656	1.64	Sb	14.90	14.89	11.71
160050.....	...	8076	12 55 25.60	29 55 29.0	1.05	0.71	2496	NGC 4794	NGC 4794	...	Sc	15.20	14.86	13.01
160055.....	4848	8082	12 55 40.69	28 30 44.4	1.51	0.58	7164	A1656	A1656	0.48	Pec	14.20	13.52	10.78
160064.....	...	...	12 56 10.19	27 32 02.6	0.64	0.58	7368	A1656	A1656	0.77	Pec/c	15.40	15.80	13.32
160067.....	...	...	12 56 12.00	27 26 47.0	0.56	0.52	7653	A1656	A1656	0.85	Pec/c	15.40	15.49	13.02
160073.....	...	...	12 56 40.34	27 54 49.2	0.79	0.70	5554	A1656	A1656	0.38	Pec/c	15.10	15.09	12.59
160076.....	...	...	12 57 15.76	28 54 01.1	0.64	0.60	5321	A1656	A1656	0.65	Sc	15.60	15.74	13.63
130003.....	...	...	12 57 20.32	22 04 55.5	1.05	0.50	7147	Isolated	Isolated	6.17	Sb	15.40	14.21	10.99
160081.....	4892	8108	12 57 38.69	27 10 01.1	1.90	0.32	5898	A1656	A1656	1.08	Sb	14.70	13.62	10.50
160086.....	...	...	12 58 08.87	27 54 23.1	0.75	0.54	7476	A1656	A1656	0.37	Irr	15.40	15.45	13.16
160088.....	IC 842	8118	12 58 15.47	29 17 19.9	1.12	0.64	7287	A1656	A1656	1.05	Sb	14.60	14.33	11.06
160260 S	...	...	12 58 29.60	28 03 09.0	...	...	...	A1656	A1656?	0.30	S0	...	...	...
160260.....	4911	8128	12 58 31.50	28 03 34.0	1.89	1.50	7912	A1656	A1656	0.30	Sa	13.70	13.48	10.02
160098.....	...	...	12 59 00.87	28 57 12.0	0.70	0.64	8762	A1656	A1656	0.78	Pec	15.30	15.29	12.19
160095.....	4921	8134	12 59 01.50	28 09 17.3	2.28	2.23	5450	A1656	A1656	0.35	Sb	13.70	13.42	9.46
160097.....	4923	...	12 59 07.40	28 06 52.0	1.15	0.83	5446	A1656	A1656	0.38	S0	14.70	14.65	11.03
160107.....	...	...	12 59 40.30	29 31 20.0	1.06	0.32	7246	A1656	A1656	1.36	S0a	14.90	14.51	10.66
160128.....	...	...	13 01 58.90	29 04 43.0	0.63	0.62	8066	A1656	A1656	1.29	Pec	15.30	15.47	13.50
160127.....	...	...	13 02 02.19	27 34 21.1	0.95	0.64	5523	A1656	A1656	1.21	Sc	15.50	15.23	13.27
130006.....	...	...	13 02 51.25	26 13 30.6	0.68	0.61	6521	Isolated	A1656	2.35	Sbc	15.00	14.87	12.09
160139.....	...	...	13 04 14.62	29 07 00.8	1.22	0.64	4748	A1656?	Isolated	1.71	Irr	15.00	14.61	13.07
160146.....	...	...	13 05 50.40	27 46 55.0	0.96	0.80	7385	A1656	A1656	1.90	Sa	15.40	15.22	11.86
130021.....	...	...	13 11 21.70	25 14 47.8	0.97	0.75	7163	Isolated	A1656	4.31	Sa	15.40	14.88	11.46
160168.....	5041	8319	13 12 11.25	30 58 12.3	1.39	1.18	7476	Isolated	Isolated	4.19	Sc	14.20	14.07	10.98
160192.....	5081	8366	13 16 46.56	28 46 06.8	2.06	0.90	6656	Isolated	A1656	4.27	Sb	14.30	13.47	10.23
101043.....	...	8437	13 22 54.62	18 42 43.3	1.36	0.30	6677	Isolated	Isolated	11.17	Sa	15.00	14.17	10.60
101054.....	5158	8459	13 25 21.31	18 02 13.1	1.40	1.30	6606	Isolated	Isolated	12.05	Sab	13.80	14.02	10.63
161063.....	...	8466	13 26 07.00	31 04 27.0	1.30	0.75	7300	Isolated	Isolated	6.83	Pec	15.50	14.73	12.25
131009.....	...	...	13 29 00.44	25 52 34.3	0.90	0.80	7522	Isolated	Isolated	7.40	Sc	15.30	15.03	12.36
108085.....	...	...	16 01 12.70	19 17 50.0	0.63	0.24	4590	FG Her	FG Her	...	Irr	15.50	15.46	13.07
224004.....	6131	10356	16 20 07.60	39 02 57.0	1.10	1.10	5094	FG Her	FG Her	...	Sc	14.20	14.31	11.51
224004 S	...	...	16 20 15.30	39 01 57.0	...	...	...	FG Her?	FG Her?	...	Sc	...	...	...
224038.....	...	10407	16 26 48.33	41 19 41.4	0.77	0.70	8446	A2197	A2197	0.47	Pec/ms	14.30	14.28	11.52

Note.—Units of right ascension are hours, minutes, and seconds, and units of declination are degrees, arcminutes, and arcseconds.

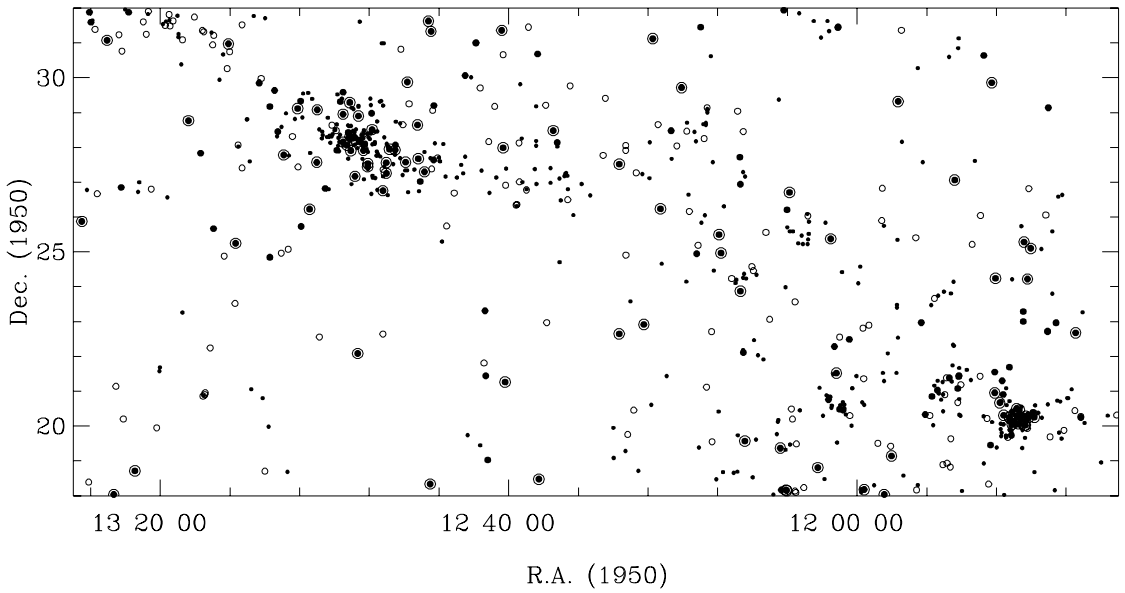

FIG. 1.—Sky distribution of CGCG galaxies that are members of the Coma supercluster (5000 km $s^{-1} < V <$ 10,000 km s^{-1}). Dots represent E + S0 galaxies, open circles spiral galaxies. Filled circles are spirals with an Hα measurement from the literature. Circled filled symbols indicate galaxies observed in the present work.

3. OBSERVATIONS AND DATA REDUCTION

Narrowband imaging of the Hα line emission ($\lambda = 6562.8$ Å) from the target galaxies was obtained from 1993 to 1997, using the 2.1 m telescope at San Pedro Mártir Observatory (SPM; Baja California, Mexico). Four galaxies were observed in 1990 using the Steward 2.3 m telescope at Kitt Peak (STW; see also Gavazzi et al. 1995a). The STW telescope was equipped with a 380 × 400 pixel CCD coupled with a focal reducer, with a resulting pixel size of 1.″2. The SPM Cassegrain focus (f/7.5) was coupled with a 1024 × 1024 pixel Thomson THX 31156 CCD in 1993 and 1994, with 0.″25 $pixel^{-1}$ and a gain of 2.12 e^- ADU^{-1}. In 1995 the system was upgraded with a 1024 × 1024 pixel Tektronix TK1024AB CCD with nearly double quantum efficiency, 0.″30 $pixel^{-1}$, and a gain of 4.88 e^- ADU^{-1}.

Each galaxy was observed using two narrowband interferometric filters: one that included the redshifted wavelength of the Hα line ("on"), the other, of similar bandwidth, centered at least 100 Å off the line ("off") to secure the continuum measurement. The flux from the [N II] emission lines (λ6548 and λ6584) is included in the on-band observations. Figure 2 shows the transmission profiles of the filters used (as provided by the manufacturer for $T = 20$°C). Figure 2*a* refers to the 1990–1995 data. The transmission curves of the SPM filters were remeasured in 1996 and are presented in Figure 2*b*. These show a slightly lower transmission than previously measured. We allowed for a transmission shift toward the blue of 1 Å per 5°C of temperature decrease. Since we observed with a dome temperature of around 10°C, we applied a 2 Å correction. At the redshift of the target galaxies, the Hα line lies well within the region of maximum filter transmission.

Table 2 reports the journal of observations as follows:

Column (*1*).—CGCG galaxy name.

Columns (*2*), (*3*).—Central wavelength of the filters used, on-band and off-band, respectively.

Column (*4*).—FWHM of the bandpass.

Column (*5*).—Telescope used.

Column (*6*).—Pixel scale.

Column (*7*).—Observing date.

Column (*8*).—Integration time per filter.

Column (*9*).—A flag indicating whether the frame was taken under photometric conditions. Galaxies marked "N" were observed in nearly photometric conditions.

Column (*10*).—Normalization factor obtained by dividing the flux of several field stars in the off-band frames by the flux in the on-band frames. In photometric conditions, this quantity reflects the transmission difference between the on- and off-band filters and ranges between 0.95 and 1.20 (for the various filters and years). Under non-photometric conditions the quantity includes variations in the sky transparency.

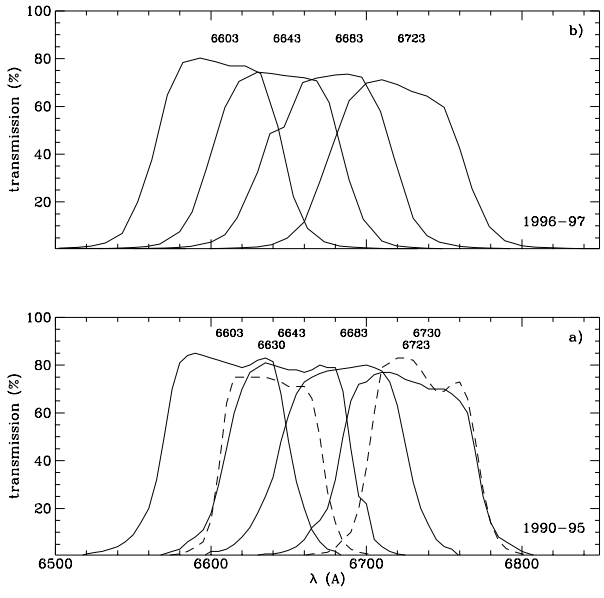

FIG. 2.—Filter transmission profiles: (*a*) 1990–1995, (*b*) 1996–1997

TABLE 2

OBSERVATION PARAMETERS

CGCG (1)	On (Å) (2)	Off (Å) (3)	$\Delta\lambda$ (Å) (4)	Telescope (5)	Pixel (″) (6)	Date (7)	T_{int} (minutes) (8)	Phot.? (9)	Norm. (10)
97073	6730	6630	70	STW	1.20	1990 Mar 20	15	Y	0.90
97079	6730	6630	70	STW	1.20	1990 Mar 20	15	Y	0.90
97087	6730	6630	70	STW	1.20	1990 Mar 20	15	Y	0.90
160055	6730	6630	70	STW	1.20	1990 Mar 20	15	Y	0.90
97125	6723	6683	90	SPM	0.25	1993 Apr 25	30	N	0.85
160127	6683	6603	90	SPM	0.25	1993 Apr 25	30	Y	1.05
97114	6723	6683	90	SPM	0.25	1993 Apr 26	30	N	1.00
97124	6723	6683	90	SPM	0.25	1993 Apr 26	30	N	0.77
97138	6683	6603	90	SPM	0.25	1993 Apr 27	30	Y	1.10
160088	6723	6603	90	SPM	0.25	1993 Apr 27	30	Y	1.10
160139	6643	6603	90	SPM	0.25	1993 Apr 27	30	Y	1.00
160086	6723	6643	90	SPM	0.25	1993 Apr 29	30	Y	0.95
160128	6723	6643	90	SPM	0.25	1993 Apr 29	30	Y	1.05
159059	6723	6643	90	SPM	0.25	1993 Apr 30	30	Y	1.05
160067	6723	6643	90	SPM	0.25	1993 Apr 30	30	Y	1.00
160064	6723	6643	90	SPM	0.25	1994 Mar 30	30	Y	1.02
97073	6723	6643	90	SPM	0.25	1994 Mar 31	30	Y	1.10
160098	6723	6643	90	SPM	0.25	1994 Mar 31	30	Y	1.00
224038	6723	6643	90	SPM	0.25	1994 Apr 5	30	Y	1.00
97088	6643	6723	90	SPM	0.30	1995 Apr 1	15	Y	0.96
97093	6643	6723	90	SPM	0.30	1995 Apr 1	15	Y	0.96
97062	6723	6643	90	SPM	0.30	1995 Apr 2	15	N	1.02
97092	6723	6643	90	SPM	0.30	1995 Apr 2	15	N	1.20
160026	6723	6643	90	SPM	0.30	1995 Apr 2	15	N	1.02
160050	6603	6683	90	SPM	0.30	1995 Apr 2	10	N	1.30
159101	6723	6643	90	SPM	0.30	1995 Apr 3	15	Y	1.03
160020	6643	6723	90	SPM	0.30	1995 Apr 3	15	Y	0.96
160073	6683	6603	90	SPM	0.30	1995 Apr 3	15	Y	1.10
160026	6723	6643	90	SPM	0.30	1995 Apr 4	15	Y	1.03
160076	6683	6603	90	SPM	0.30	1995 Apr 4	15	Y	1.10
101054	6683	6603	90	SPM	0.30	1996 Apr 18	20	Y	1.08
127052	6723	6603	90	SPM	0.30	1996 Apr 18	20	Y	1.10
127054	6723	6603	90	SPM	0.30	1996 Apr 18	20	Y	1.08
158036	6683	6603	90	SPM	0.30	1996 Apr 18	20	Y	1.20
160024	6723	6603	90	SPM	0.30	1996 Apr 18	20	Y	1.15
160025	6723	6603	90	SPM	0.30	1996 Apr 18	20	Y	1.15
160095	6683	6603	90	SPM	0.30	1996 Apr 18	20	Y	1.10
160097	6683	6603	90	SPM	0.30	1996 Apr 18	20	Y	1.10
97129 E.....	6683	6603	90	SPM	0.30	1996 Apr 19	20	Y	1.10
97129 W.....	6683	6603	90	SPM	0.30	1996 Apr 19	20	Y	1.10
128089	6723	6603	90	SPM	0.30	1996 Apr 19	20	Y	1.20
159008	6723	6603	90	SPM	0.30	1996 Apr 19	20	Y	1.20
159102	6723	6603	90	SPM	0.30	1996 Apr 19	20	Y	1.10
160081	6683	6603	90	SPM	0.30	1996 Apr 19	20	Y	1.08
160168	6723	6603	90	SPM	0.30	1996 Apr 19	20	Y	1.10
160192	6723	6603	90	SPM	0.30	1996 Apr 19	20	Y	1.10
160260	6723	6603	90	SPM	0.30	1996 Apr 19	20	Y	1.10
160260 S.....	6723	6603	90	SPM	0.30	1996 Apr 19	20	Y	1.10
161063	6723	6603	90	SPM	0.30	1996 Apr 19	20	Y	1.08
98058	6723	6603	90	SPM	0.30	1996 Apr 20	20	Y	1.08
98116	6683	6603	90	SPM	0.30	1996 Apr 20	20	Y	1.08
128073	6723	6603	90	SPM	0.30	1996 Apr 20	20	Y	1.10
129020	6683	6603	90	SPM	0.30	1996 Apr 20	20	Y	1.20
131009	6723	6603	90	SPM	0.30	1996 Apr 20	20	Y	1.10
157064	6683	6603	90	SPM	0.30	1996 Apr 20	20	Y	1.10
159061	6723	6603	90	SPM	0.30	1996 Apr 20	20	Y	1.08
159095	6723	6603	90	SPM	0.30	1996 Apr 20	20	Y	1.08
160005	6683	6603	90	SPM	0.30	1996 Apr 20	20	Y	1.10
97078	6723	6603	90	SPM	0.30	1996 Apr 21	20	Y	1.10
97082	6723	6603	90	SPM	0.30	1996 Apr 21	20	Y	1.10
97102 N	6683	6603	90	SPM	0.30	1996 Apr 21	20	Y	1.08
97102 S	6683	6603	90	SPM	0.30	1996 Apr 21	20	Y	1.08
101043	6723	6603	90	SPM	0.30	1996 Apr 21	20	Y	1.10
130006	6683	6603	90	SPM	0.30	1996 Apr 21	20	Y	1.10
158105	6723	6603	90	SPM	0.30	1996 Apr 21	20	Y	1.08
159033	6723	6603	90	SPM	0.30	1996 Apr 21	20	Y	1.10
159096	6683	6603	90	SPM	0.30	1996 Apr 21	20	Y	1.10
160032	6723	6603	90	SPM	0.30	1996 Apr 21	20	Y	1.08
160107	6723	6603	90	SPM	0.30	1996 Apr 21	20	Y	1.10
108085	6683	6603	90	SPM	0.30	1996 Apr 21	15	Y	1.08
224004	6683	6603	90	SPM	0.30	1996 Apr 21	12	Y	1.07

TABLE 2—*Continued*

CGCG (1)	On (Å) (2)	Off (Å) (3)	$\Delta\lambda$ (Å) (4)	Telescope (5)	Pixel (″) (6)	Date (7)	T_{int} (minutes) (8)	Phot.? (9)	Norm. (10)
224004 S.....	6683	6603	90	SPM	0.30	1996 Apr 21	12	Y	1.07
119055	6683	6603	90	SPM	0.30	1997 Mar 8	20	Y	1.08
119109	6643	6723	90	SPM	0.30	1997 Mar 8	20	Y	0.96
98013	6723	6603	90	SPM	0.30	1997 Mar 8	20	N	1.20
98023	6723	6603	90	SPM	0.30	1997 Mar 8	20	Y	1.08
98078	6723	6603	90	SPM	0.30	1997 Mar 8	20	Y	1.08
98081	6723	6603	90	SPM	0.30	1997 Mar 8	20	Y	1.08
100012	6723	6603	90	SPM	0.30	1997 Mar 8	20	Y	1.08
127033	6683	6603	90	SPM	0.30	1997 Mar 8	20	Y	1.08
128066	6723	6603	90	SPM	0.30	1997 Mar 8	20	Y	1.08
129004	6723	6603	90	SPM	0.30	1997 Mar 8	20	Y	1.08
157032	6723	6603	90	SPM	0.30	1997 Mar 8	20	Y	1.08
160018	6723	6603	90	SPM	0.30	1997 Mar 8	20	Y	1.08
160146	6723	6603	90	SPM	0.30	1997 Mar 8	20	Y	1.08
119035	6603	6723	90	SPM	0.30	1997 Mar 9	20	Y	0.93
119078	6603	6723	90	SPM	0.30	1997 Mar 9	20	Y	0.93
98016	6723	6603	90	SPM	0.30	1997 Mar 9	20	Y	1.08
98087	6723	6603	90	SPM	0.30	1997 Mar 9	20	Y	1.08
127005	6723	6603	90	SPM	0.30	1997 Mar 9	20	Y	1.08
128015	6723	6603	90	SPM	0.30	1997 Mar 9	20	Y	1.08
128087	6723	6603	90	SPM	0.30	1997 Mar 9	20	Y	1.08
158094	6723	6603	90	SPM	0.30	1997 Mar 9	20	Y	1.08
159097	6723	6603	90	SPM	0.30	1997 Mar 9	20	Y	1.08
160007	6723	6603	90	SPM	0.30	1997 Mar 9	20	Y	1.08
119093	6643	6723	90	SPM	0.30	1997 Mar 10	20	Y	0.96
119096	6723	6603	90	SPM	0.30	1997 Mar 10	20	Y	1.08
99104	6723	6603	90	SPM	0.30	1997 Mar 10	20	Y	1.08
127037	6683	6603	90	SPM	0.30	1997 Mar 10	20	Y	1.08
127035	6723	6603	90	SPM	0.30	1997 Mar 10	20	Y	1.08
127053	6683	6603	90	SPM	0.30	1997 Mar 10	20	Y	1.08
128021	6723	6603	90	SPM	0.30	1997 Mar 10	20	Y	1.08
128072	6723	6603	90	SPM	0.30	1997 Mar 10	20	Y	1.08
130003	6723	6603	90	SPM	0.30	1997 Mar 10	20	Y	1.08
130021	6723	6603	90	SPM	0.30	1997 Mar 10	20	Y	1.08
157044	6723	6603	90	SPM	0.30	1997 Mar 10	20	Y	1.08

All images were obtained in seeing conditions in the range 1.″3–2.″5.

3.1. *Image Analysis*

The data reduction of the present frames was based on the IRAF package, developed by NOAO, and on the SAOIMAGE package, developed at CfA. To remove the detector response, every raw image was bias-subtracted and divided by the flat field obtained from the twilight sky. Cosmic rays were individually removed from each frame. Bad pixel columns were removed by direct inspection of the frames and replaced with the mean of adjacent columns. The sky background was determined in each frame in concentric object-free annuli about the object and then subtracted from the flat-fielded images. These resulting frames were then used to determine the total counts from the objects of interest (galaxies and stars).

Let us consider a frame containing a target galaxy (with total counts cnts^g) and one or more field stars (with total counts cnts*). Under the assumption that the field stars do not emit Hα, i.e., that

$$\mathrm{flux}^*_{\mathrm{on}}/\mathrm{flux}^*_{\mathrm{off}} = 1 ,$$

we have

$$\mathrm{cnts}^*_{\mathrm{on}}/\mathrm{cnts}^*_{\mathrm{off}} = T_{\mathrm{on}}\,\tau_{\mathrm{on}}\,c/T_{\mathrm{off}}\,\tau_{\mathrm{off}}\,c = K ,$$

where

$$\mathrm{cnts} = (\mathrm{flux})T\tau c ,$$

T is the effective integration time, τ is the integral of the filter transmission, and c is the conversion factor from counts s^{-1} to ergs $\mathrm{cm}^{-2}\,\mathrm{s}^{-1}$.

For a target galaxy, the Hα equivalent width is then

$$\mathrm{EW} = \frac{\mathrm{flux}^g_{\mathrm{on}} - \mathrm{flux}^g_{\mathrm{off}}}{\mathrm{flux}^g_{\mathrm{off}}} = \frac{\mathrm{cnts}^g_{\mathrm{on}} - K\mathrm{cnts}^g_{\mathrm{off}}}{K\mathrm{cnts}^g_{\mathrm{off}}}\ (\text{Å})$$

independent of c, and thus derivable also in non-photometric conditions from the observed quantity K. The net flux in the Hα line is given by

$$\frac{\mathrm{cnts}^g_{\mathrm{on}}}{T_{\mathrm{on}}\,\tau_{\mathrm{on}}\,c} - \frac{\mathrm{cnts}^g_{\mathrm{off}}}{T_{\mathrm{off}}\,\tau_{\mathrm{off}}\,c} = \frac{\mathrm{cnts}^g_{\mathrm{on}} - K\mathrm{cnts}^g_{\mathrm{off}}}{T_{\mathrm{on}}\,\tau_{\mathrm{on}}\,c}\ (\text{ergs cm}^{-2}\ \text{s}^{-1}) ,$$

which requires a determination of c from the calibration process.

In order to calibrate our data, we observed the spectrophotometric stars Feige 34, Hz 44 and BD +33°2642 just before or after the target galaxies. Their measured spectral energy distributions (available in IRAF in tabular form) were then convolved with the filter transmission profiles to obtain the value of c.

4. RESULTS

Figure 3*a* gives a gray-scale representation of the off (*top*) and net (on minus off, *bottom*) frames of all galaxies with a net flux. Figure 3*b* carries the off frames of 11 galaxies with null or negative net flux.

Table 3 reports the results of the present work as follows:

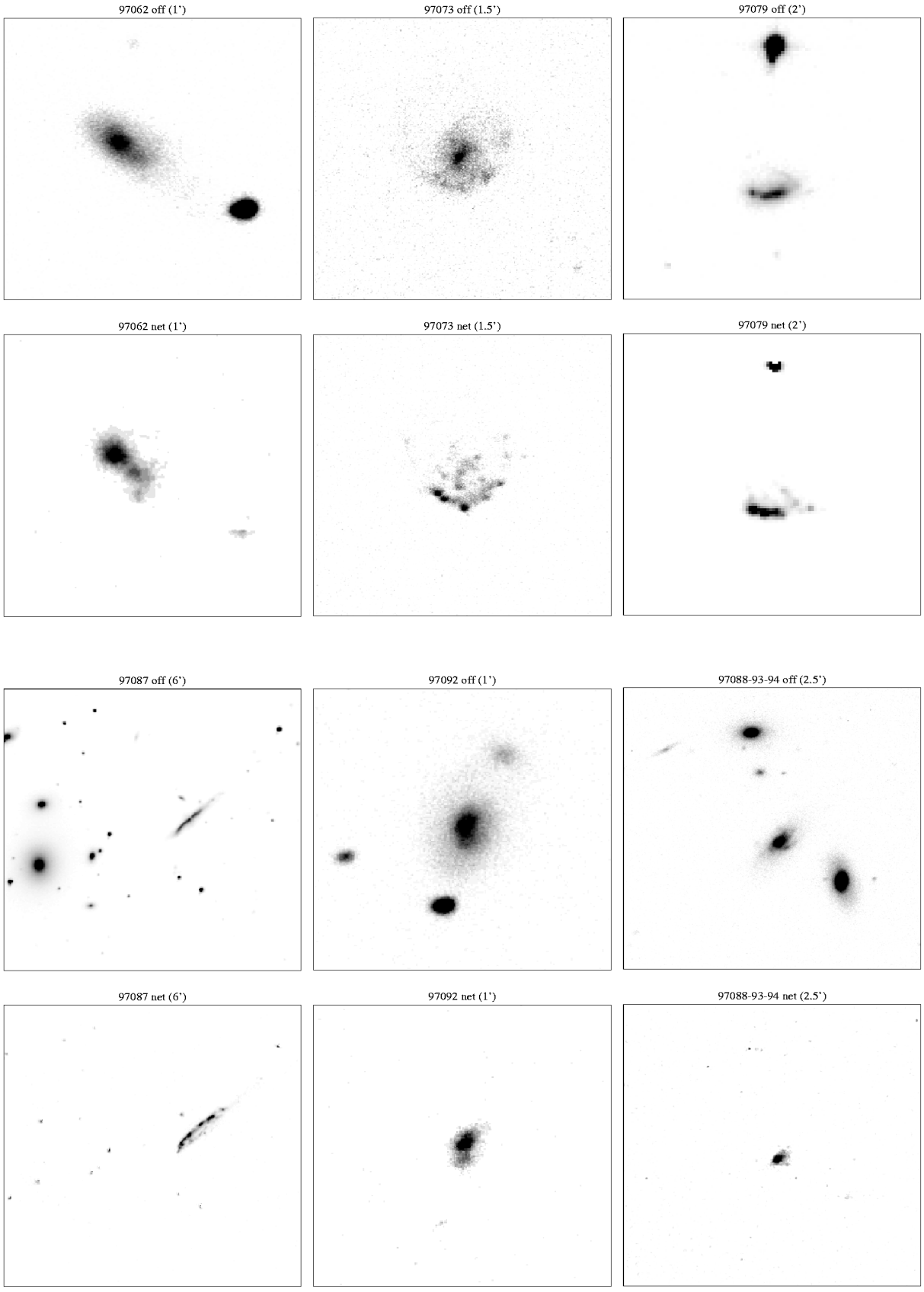

FIG. 3*a*

FIG. 3.—(*a*) Gray-scale representation of the off (*top*) and net (on minus off, *bottom*) frames of all galaxies with a net Hα flux; (*b*) off frames of 11 galaxies with null or negative net flux. The size of the displayed field is given in parentheses. North is at the top, east to the left.

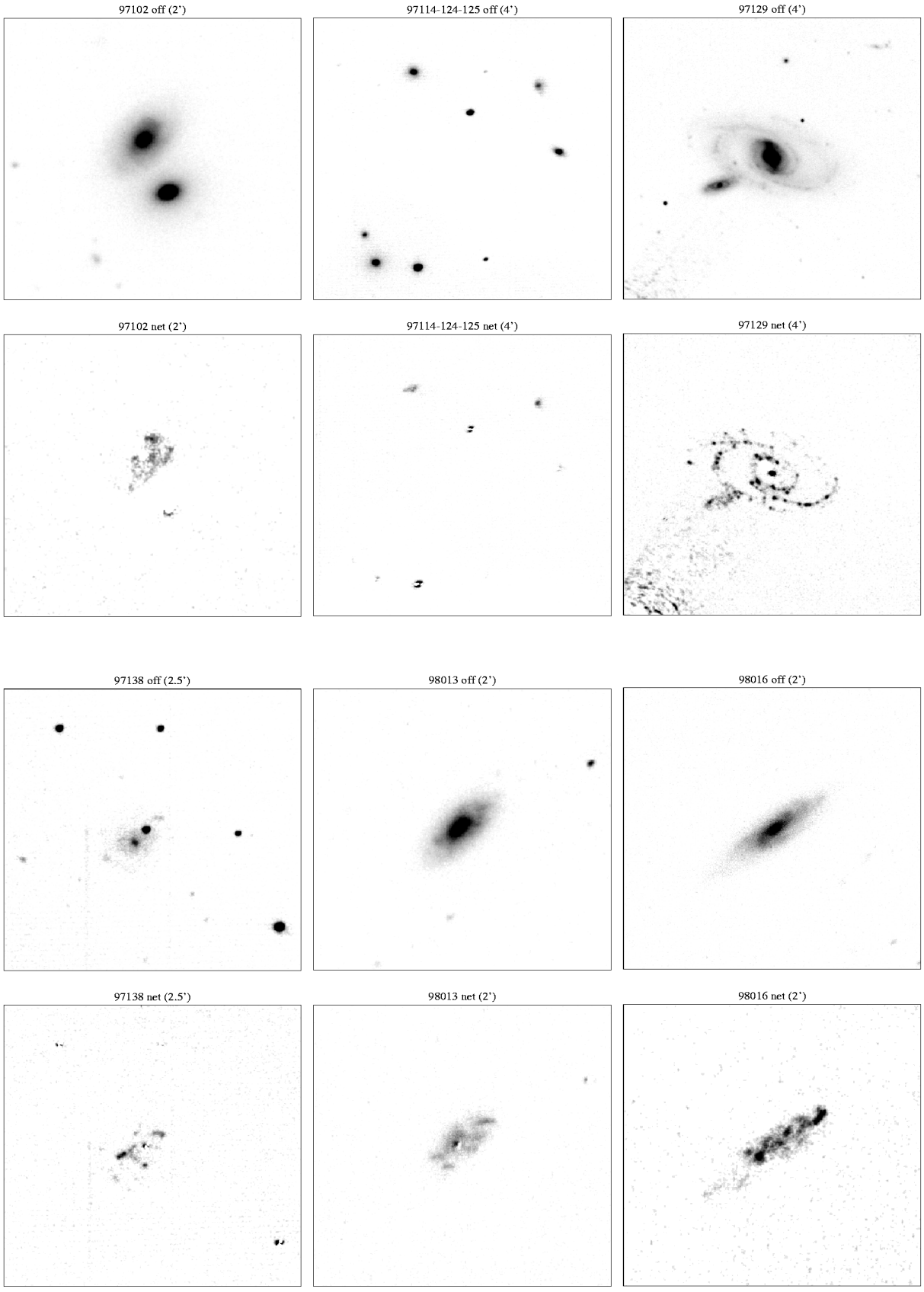

FIG. 3*a.—Continued*

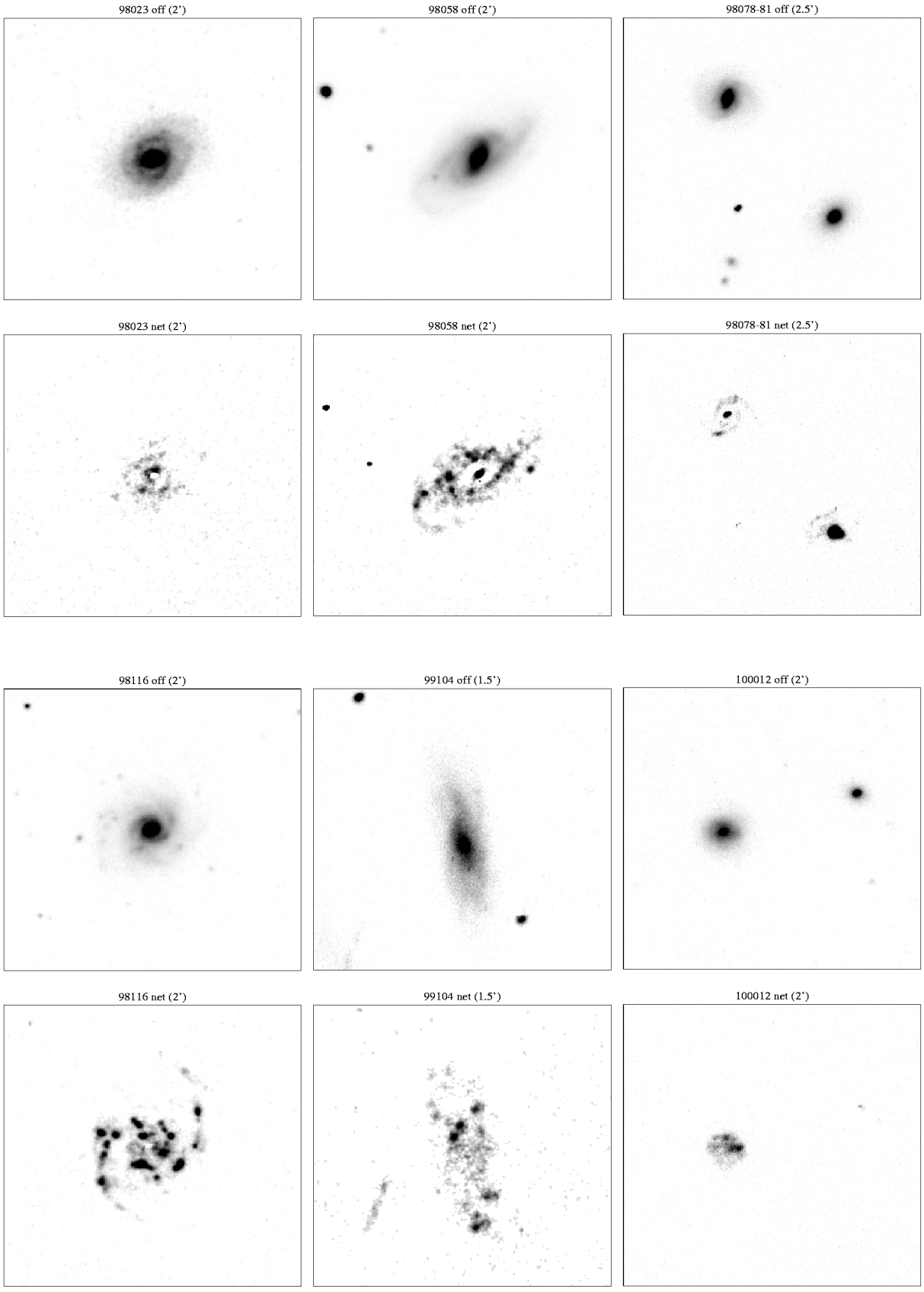

FIG. 3*a.—Continued*

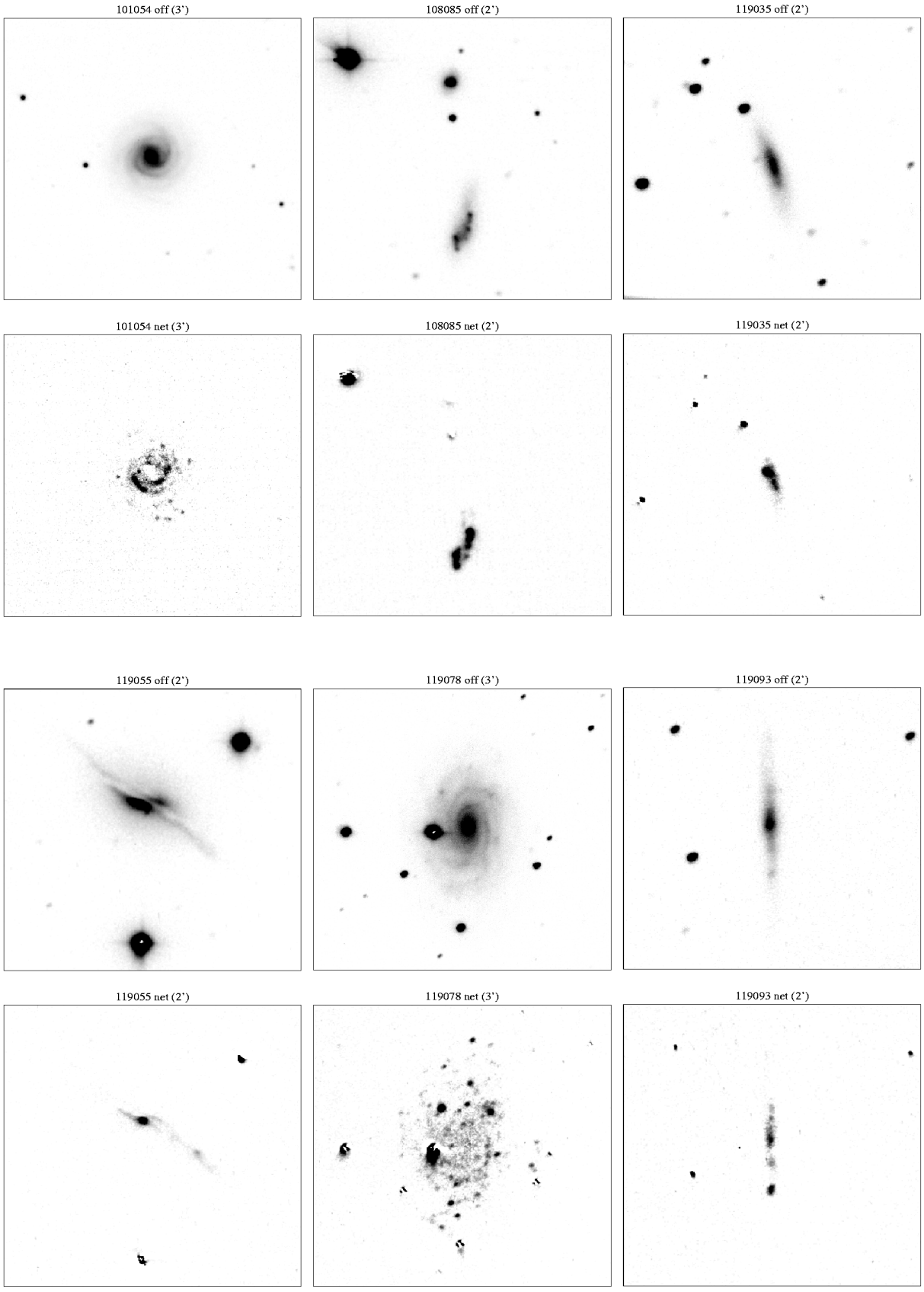

FIG. 3*a.—Continued*

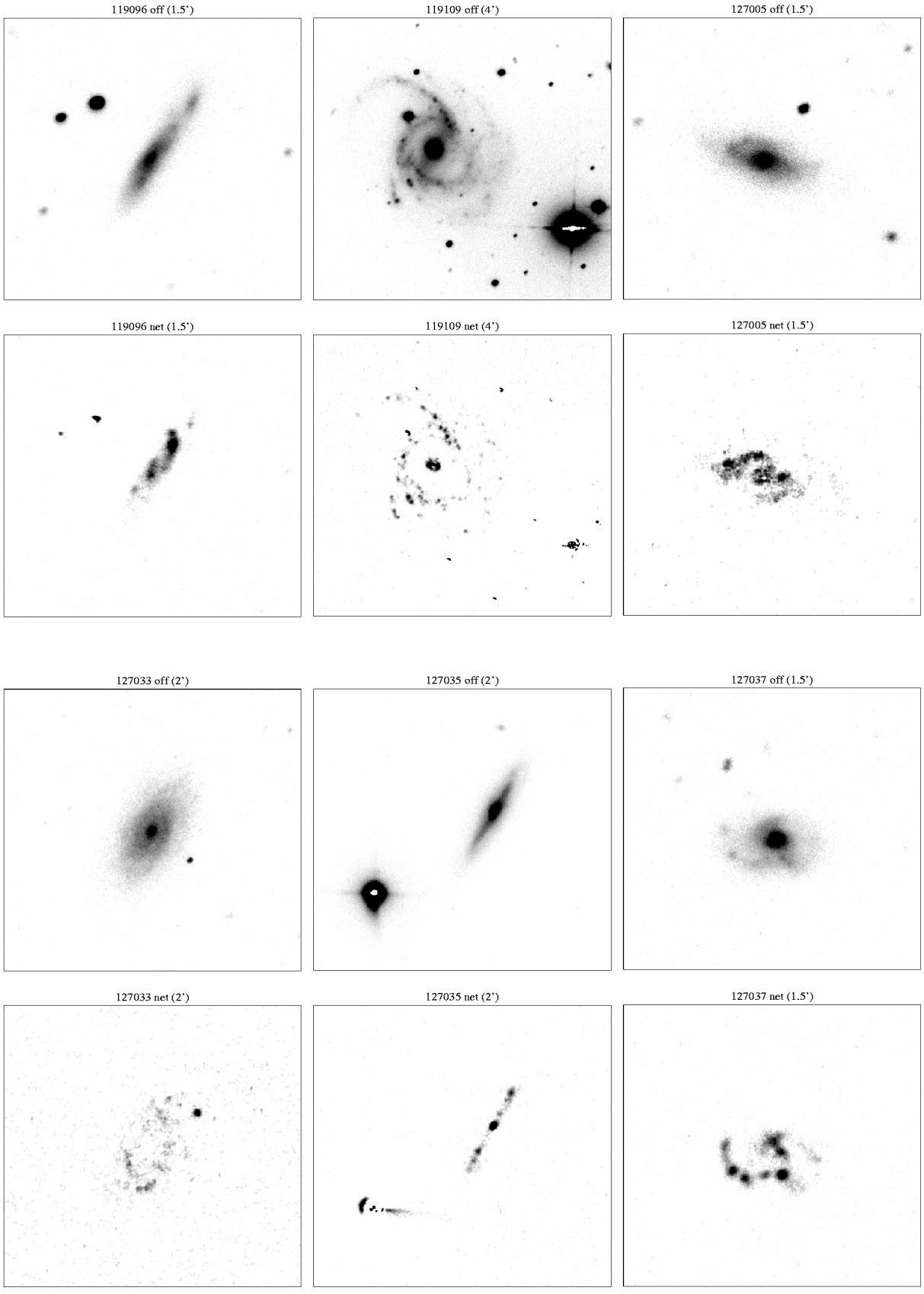

FIG. 3*a.—Continued*

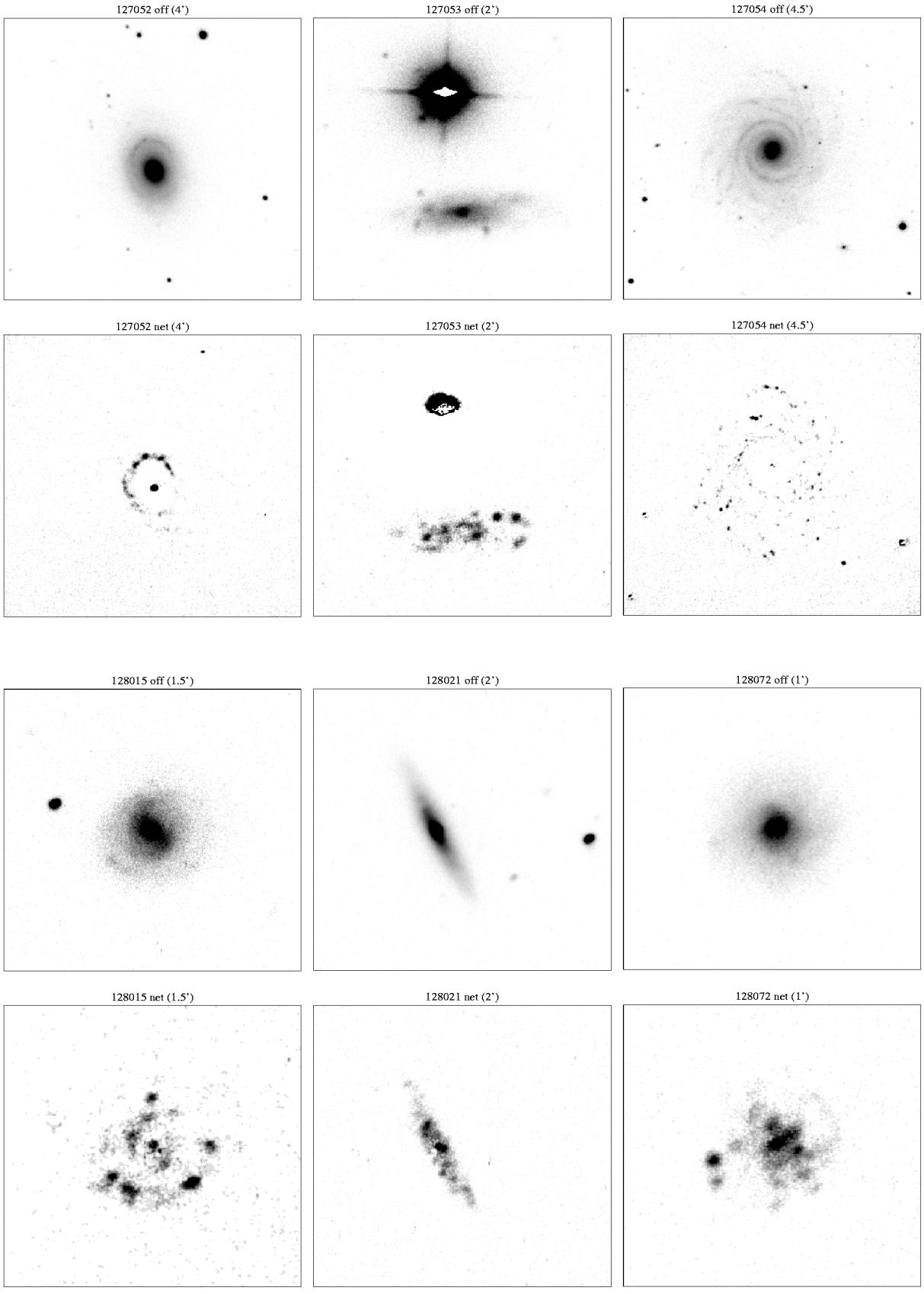

FIG. 3*a.—Continued*

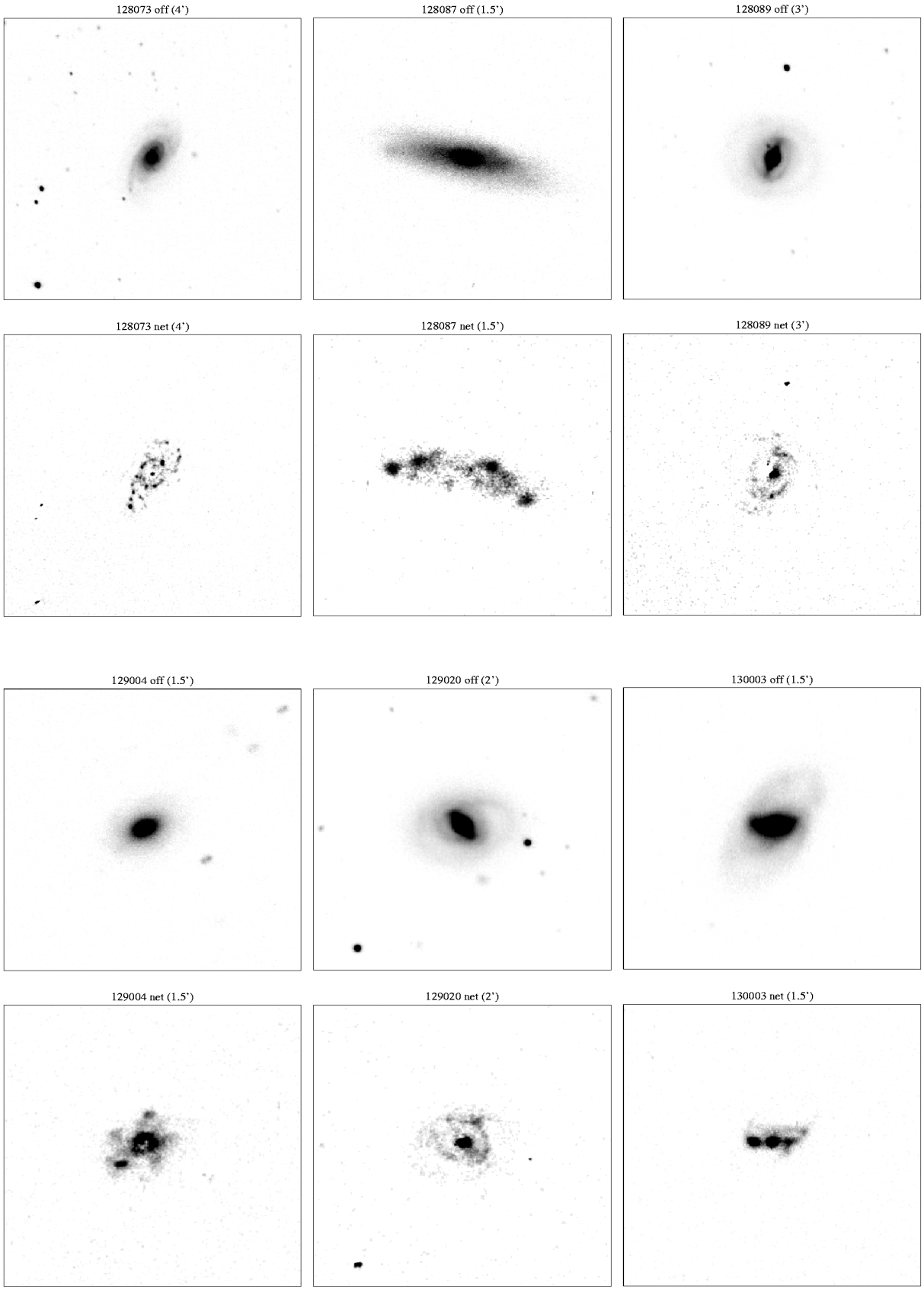

FIG. 3*a.—Continued*

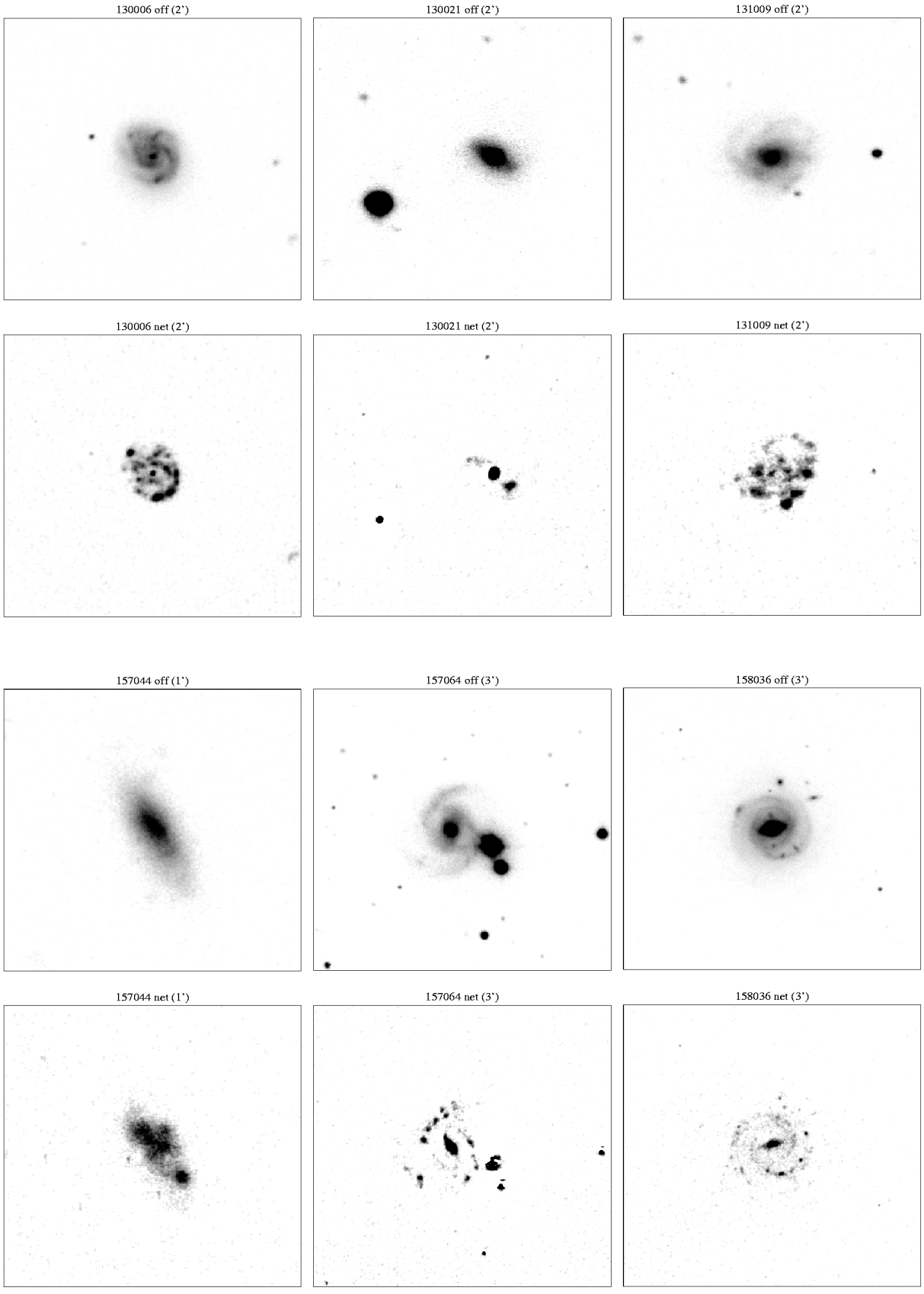

FIG. 3*a.*—*Continued*

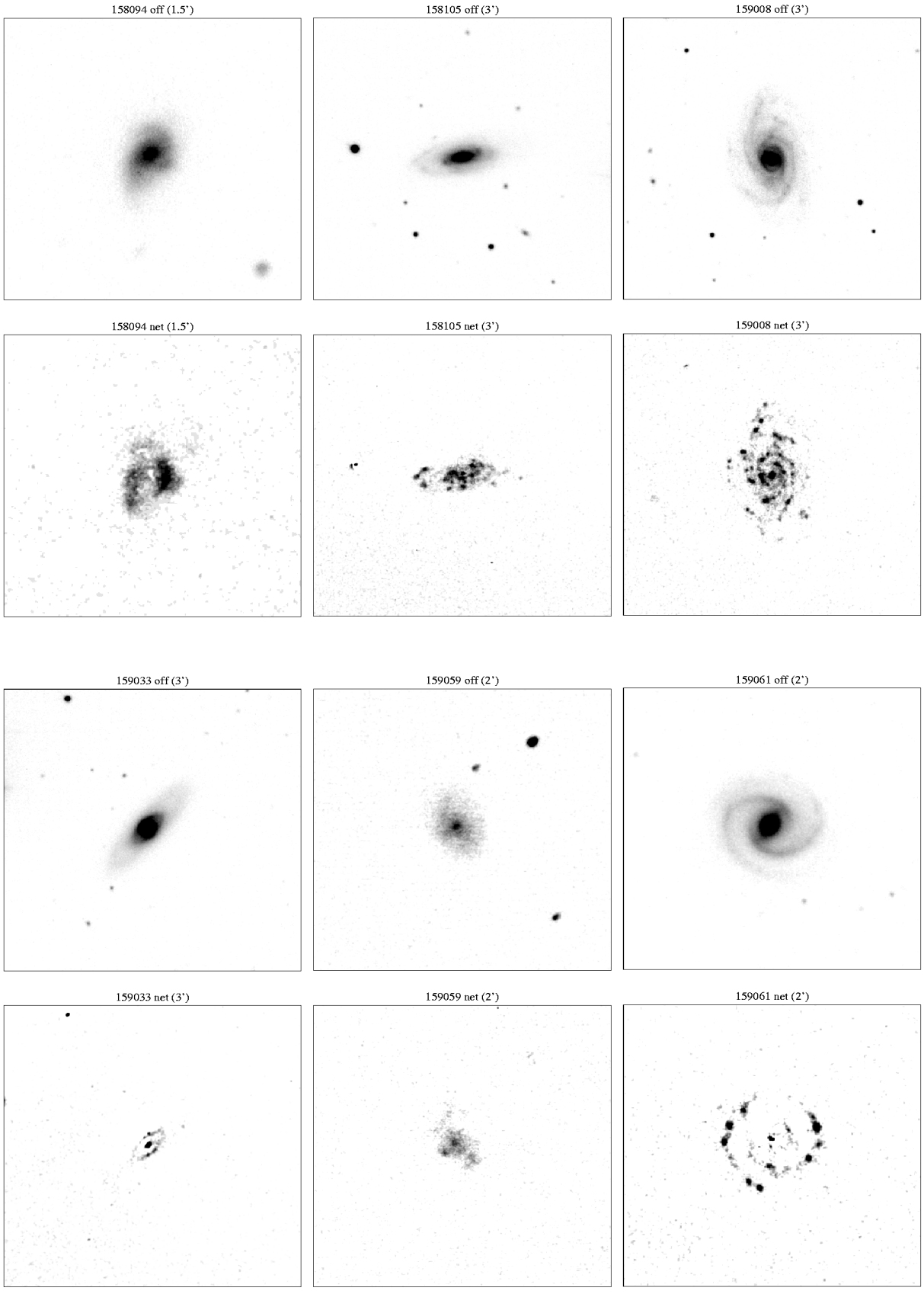

FIG. 3*a.—Continued*

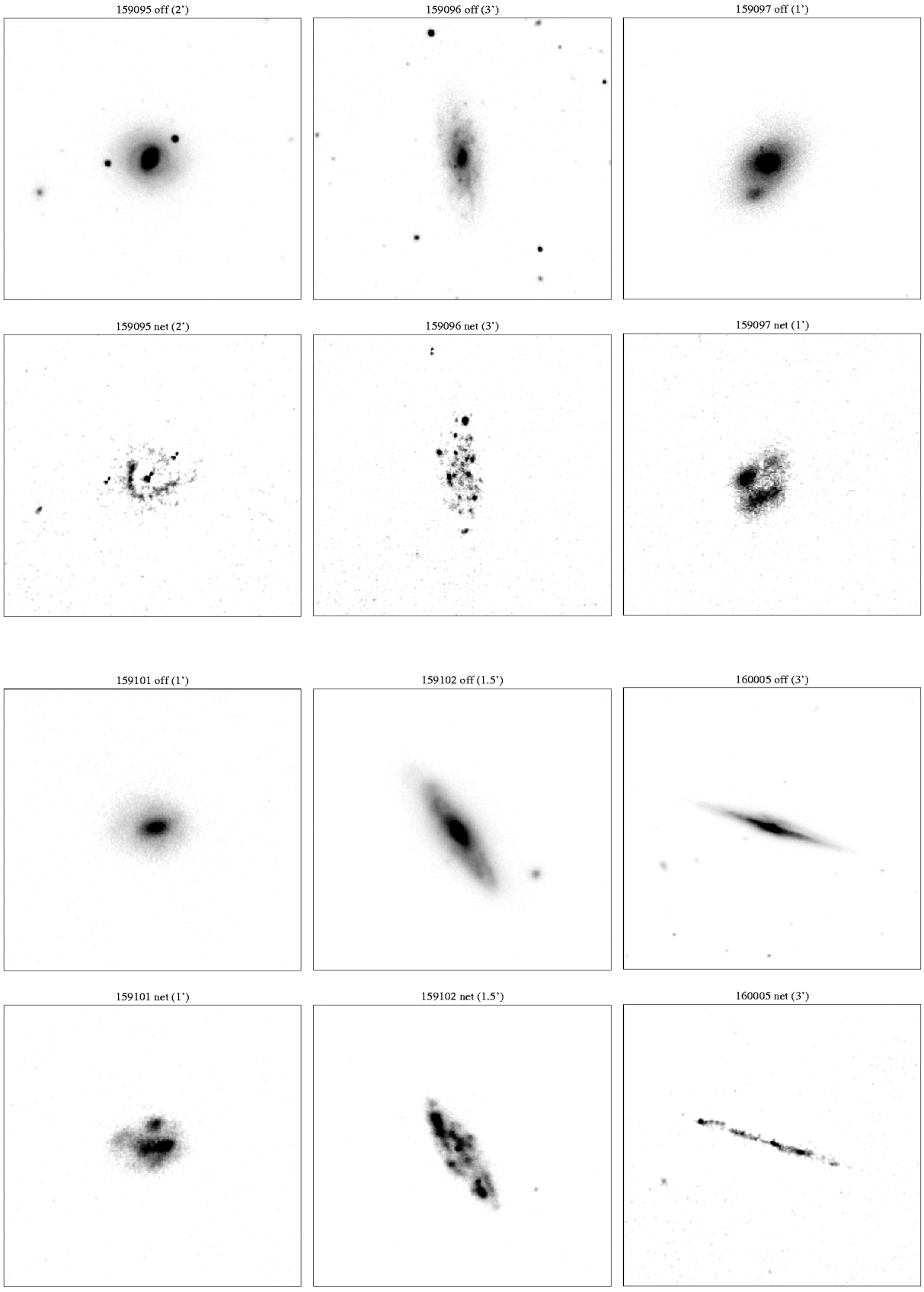

FIG. 3*a.*—*Continued*

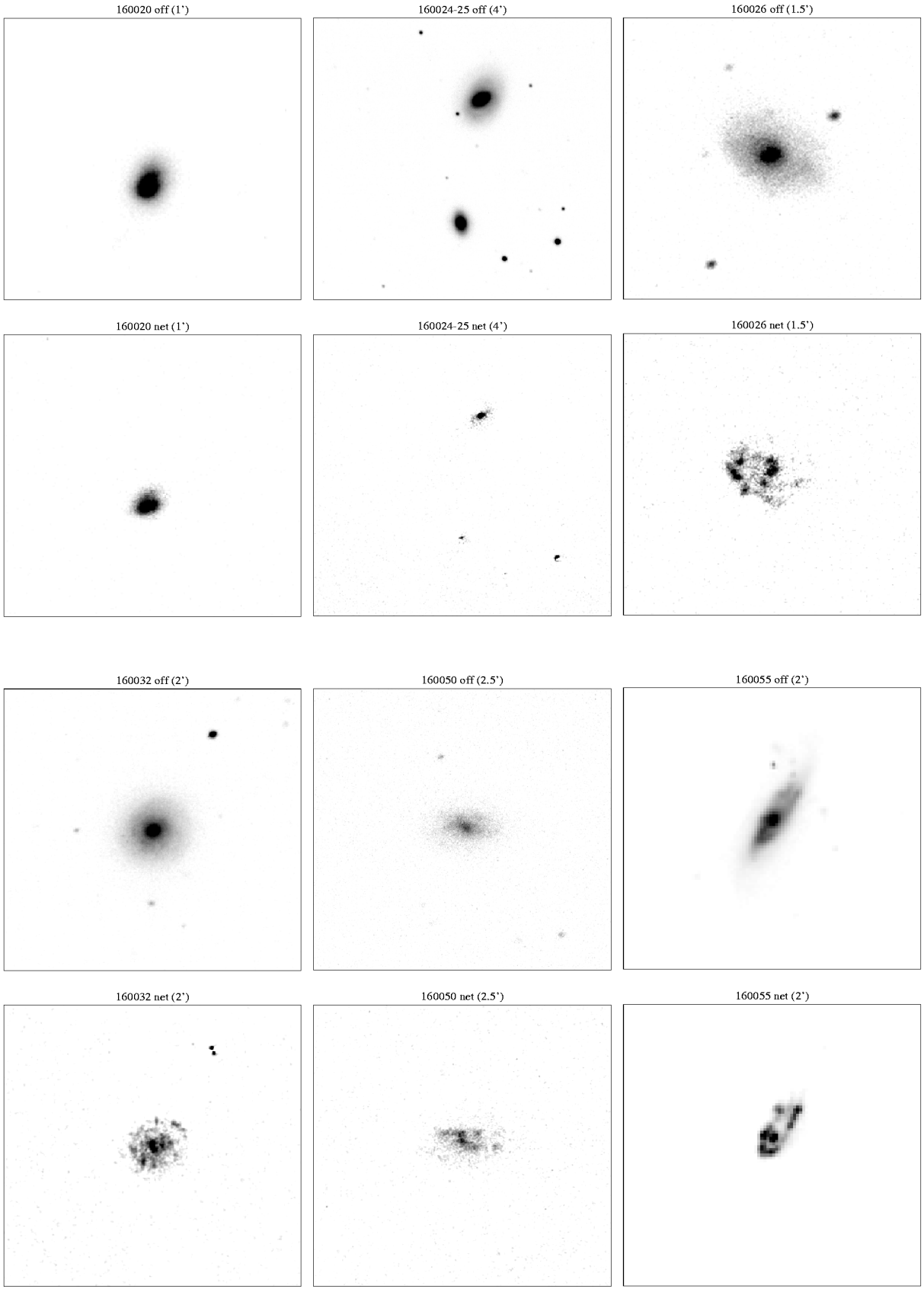

FIG. 3*a.—Continued*

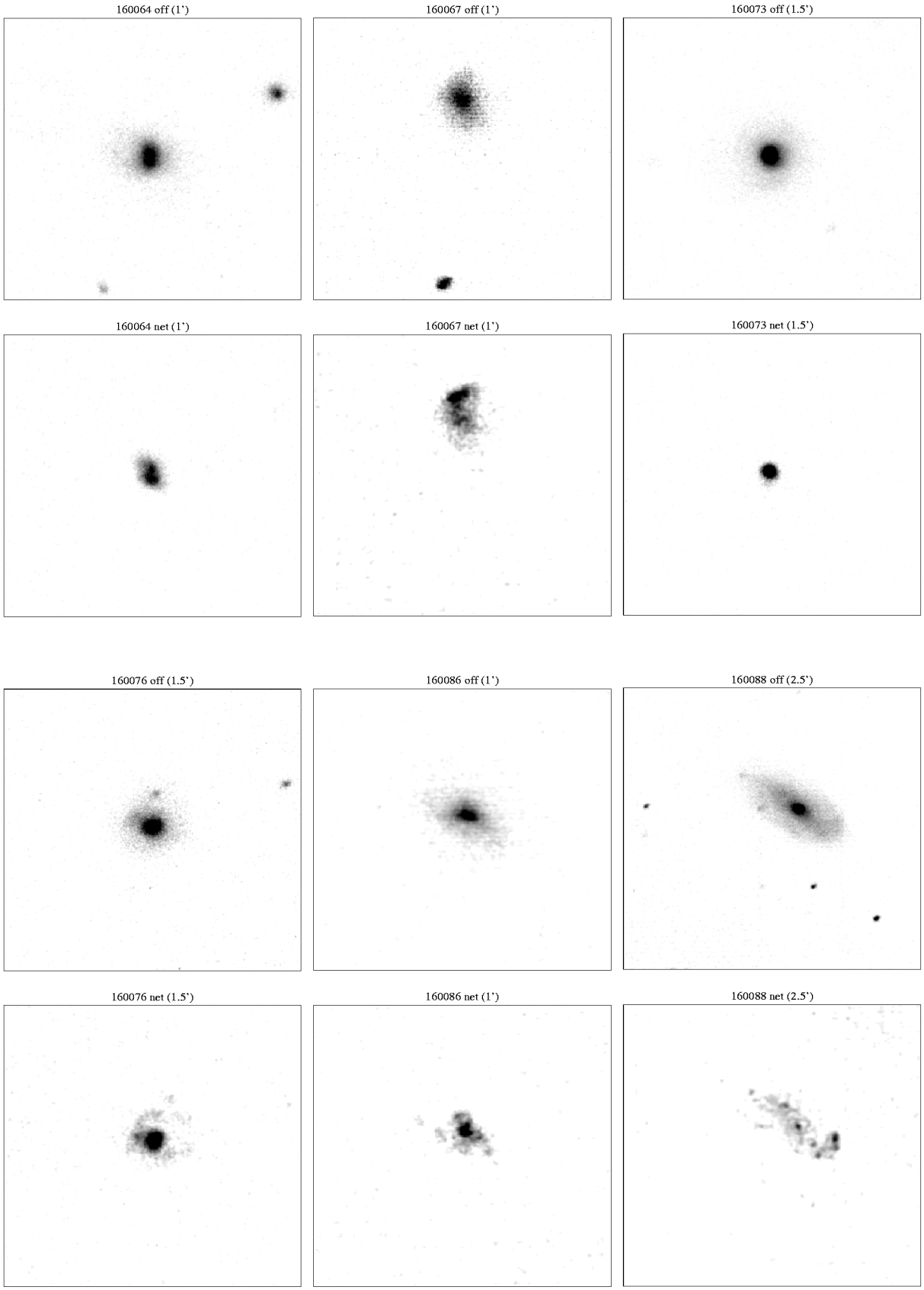

FIG. 3*a.—Continued*

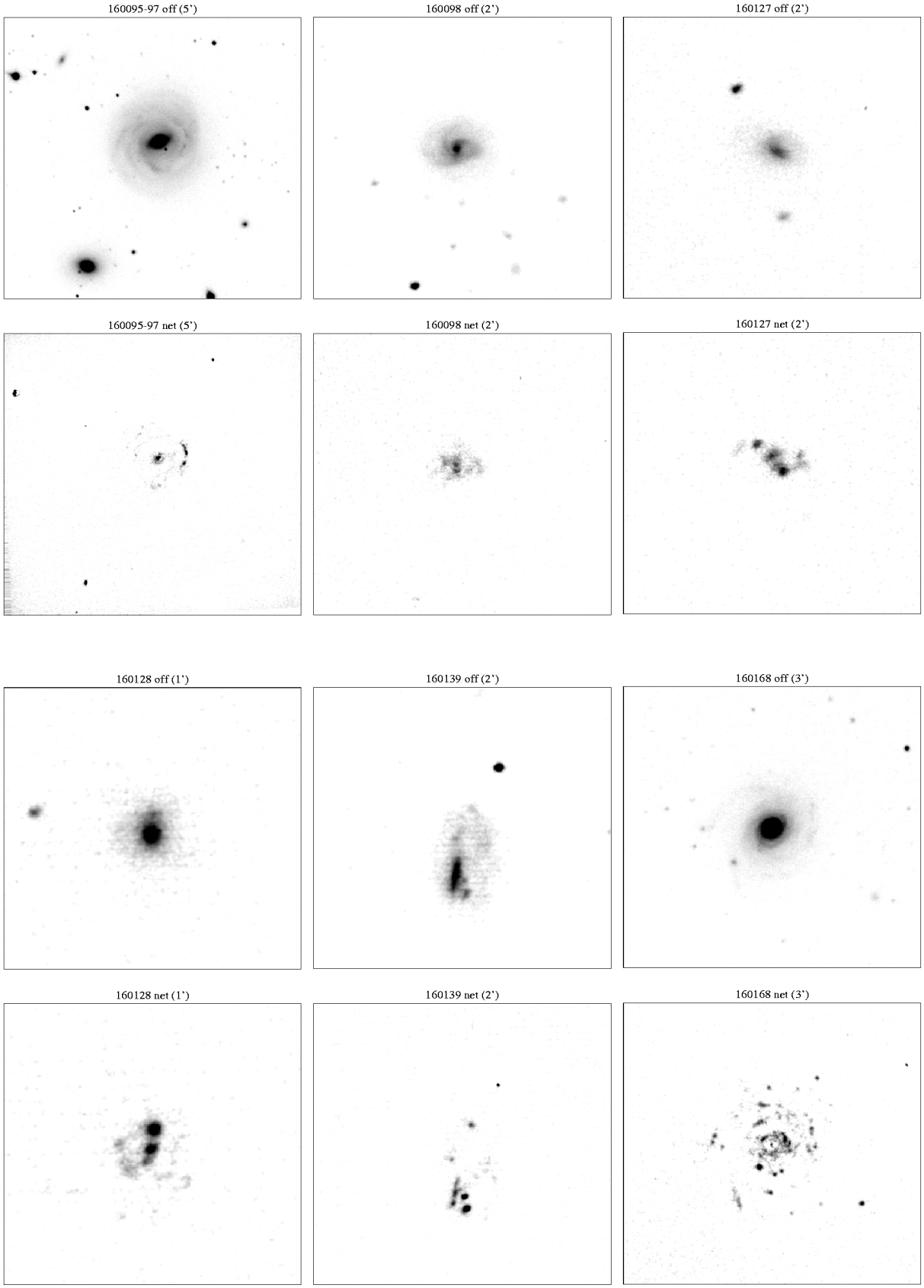

FIG. 3*a*.—*Continued*

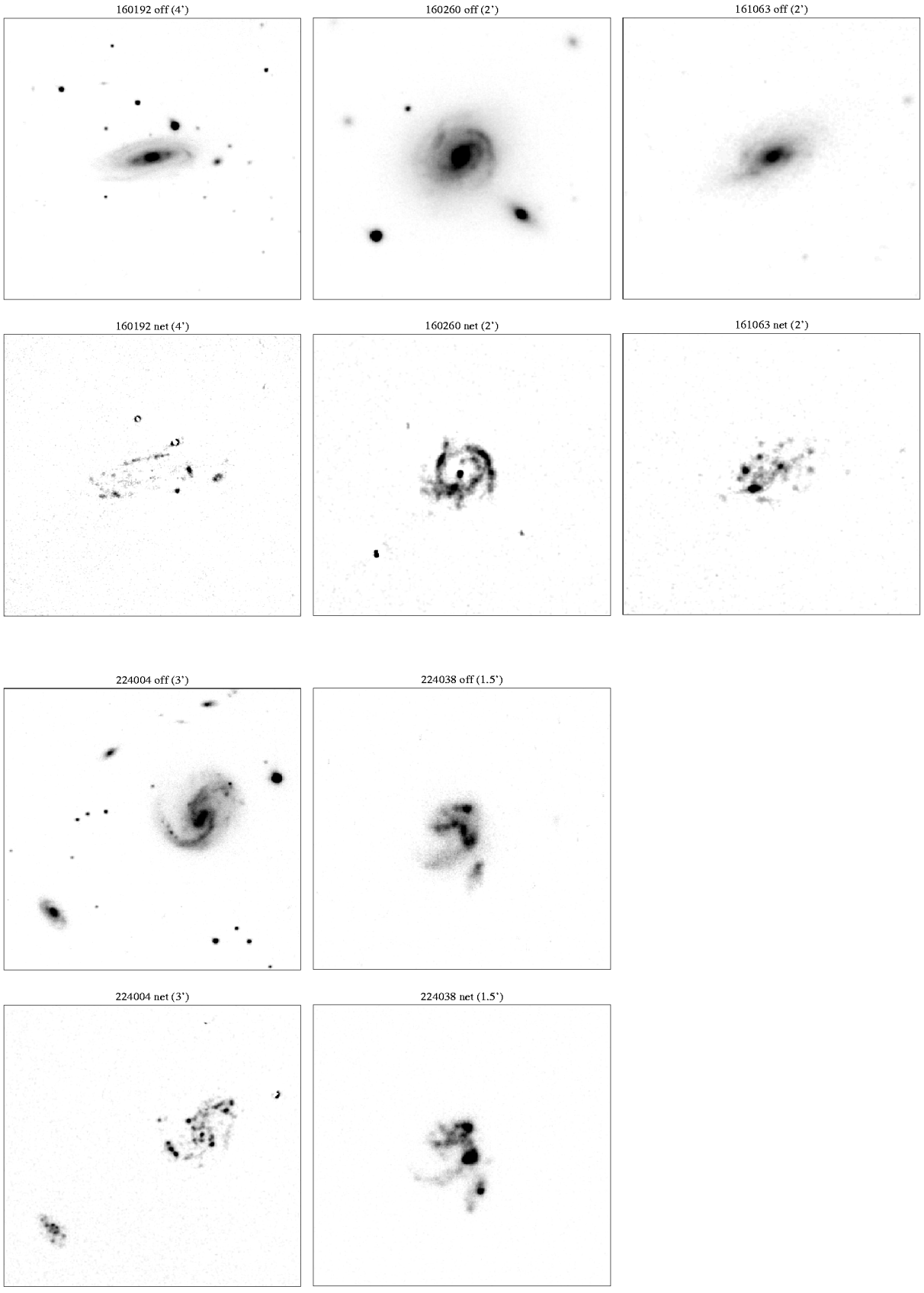

FIG. 3*a*.—*Continued*

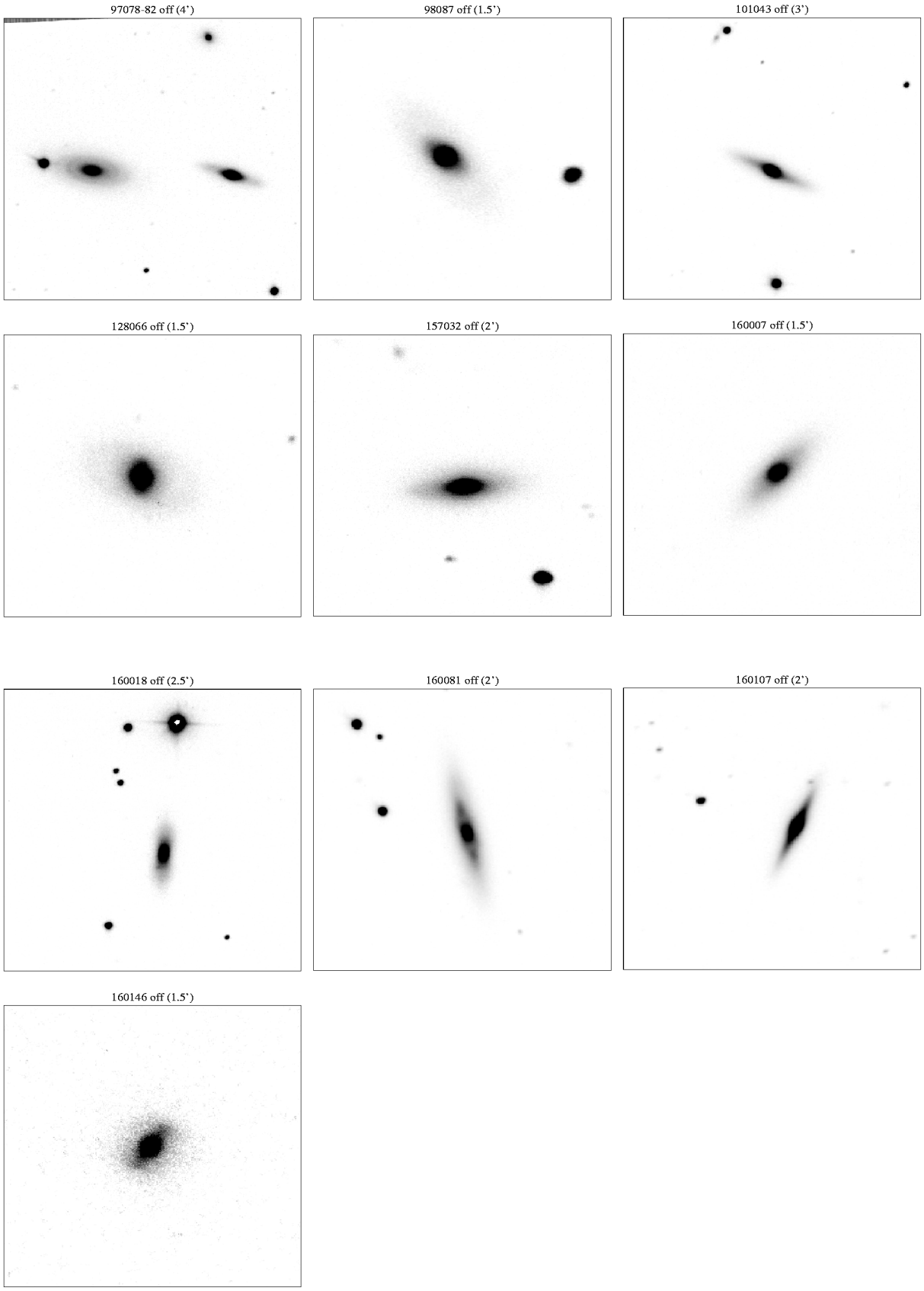
97078-82 off (4')
98087 off (1.5')
101043 off (3')
128066 off (1.5')
157032 off (2')
160007 off (1.5')
160018 off (2.5')
160081 off (2')
160107 off (2')
160146 off (1.5')

FIG. 3*b*

TABLE 3

RESULTS

		This Work			Literature		
CGCG (1)	Telescope (2)	Hα EW (Å) (3)	Hα Flux (4)	Hα Luminosity (5)	Hα EW (Å) (6)	Hα Flux (7)	Reference (8)
97062	SPM	34.2 ± 1.3	...	...	45 ± 10	−13.10	1
97073	SPM	108.1 ± 24.3	−12.76	40.95	80 ± 12	−12.84	1
97073	STW	93.9 ± 12.4	−12.75	40.95	80 ± 12	−12.84	1
97078	SPM	−2.8 ± 2.2	...	...			
97079	STW	137.1 ± 6.0	−12.66	41.04	145 ± 15	−12.64	1
97082	SPM	−3.5 ± 1.3	...	...			
97087	STW	73.7 ± 2.3	−12.22	41.48	61 ± 5	−12.19	1
97088	SPM	−1.6 ± 1.0	...	...			
97092	SPM	26.8 ± 2.7	...	...	...	−13.06	2
97093	SPM	9.8 ± 5.1	−13.62	40.09	59	−12.95	2
97102 N	SPM	2.2 ± 2.0	−13.92	39.79			
97102 S	SPM	−3.1 ± 1.2	...	...			
97114	SPM	48.2 ± 4.8	...	...	79	−12.82	2
97124	SPM	5.0 ± 7.1	...	...			
97125	SPM	20.9 ± 7.6	...	...	29 ± 4	−13.13	2
97129 E	SPM	18.0 ± 2.3	−13.38	40.32			
97129 W.....	SPM	13.9 ± 4.1	−12.54	41.16	10 ± 2	−12.58	1
97138	SPM	63.9 ± 16.6	−12.94	40.77	31 ± 4	−13.09	1
98013	SPM	34.1 ± 4.0	...	...			
98016	SPM	29.6 ± 4.7	−13.04	40.66			
98023	SPM	10.8 ± 2.3	−13.31	40.47			
98058	SPM	10.5 ± 0.8	−13.01	40.78			
98078	SPM	81.7 ± 2.8	−12.61	41.14			
98081	SPM	14.2 ± 2.6	−13.19	40.60			
98087	SPM	−0.1 ± 1.1	...	...			
98116	SPM	40.6 ± 5.3	−12.64	41.03			
99104	SPM	16.8 ± 3.5	−13.28	40.60			
100012	SPM	39.1 ± 7.6	−13.06	40.64			
101043	SPM	−3.2 ± 0.6	...	...			
101054	SPM	10.8 ± 1.4	−12.91	40.81			
108085	SPM	88.0 ± 3.3	−12.76	40.64			
119035	SPM	25.2 ± 2.9	−13.18	39.55			
119055	SPM	16.5 ± 3.0	−13.00	40.43			
119078	SPM	19.4 ± 3.4	−12.28	40.45			
119093	SPM	16.5 ± 5.7	−13.62	39.80			
119096	SPM	30.1 ± 4.5	−13.03	40.91			
119109	SPM	6.2 ± 4.0	−12.74	40.68	16 ± 3	−12.35	1
127005	SPM	26.6 ± 4.5	−13.14	40.61			
127033	SPM	10.8 ± 2.8	−13.26	40.41			
127035	SPM	9.8 ± 1.8	−13.27	40.47			
127037	SPM	47.7 ± 3.4	−12.92	40.74			
127052	SPM	4.2 ± 5.4	−13.02	40.68			
127053	SPM	16.7 ± 6.5	−13.05	40.64			
127054	SPM	4.0 ± 10.3	−13.01	40.76	5 ± 3	> −13.0	1
128015	SPM	21.5 ± 5.1	−13.09	40.65			
128021	SPM	16.1 ± 0.6	−12.99	40.78			
128066	SPM	−2.4 ± 1.9	...	...			
128072	SPM	37.0 ± 2.8	−12.97	40.78			
128073	SPM	15.4 ± 2.5	−12.95	40.82			
128087	SPM	13.9 ± 1.3	−13.15	40.58			
128089	SPM	8.8 ± 3.9	−13.11	40.64			
129004	SPM	34.1 ± 3.0	−12.93	40.83			
129020	SPM	10.4 ± 1.0	−13.12	40.60			
130003	SPM	18.4 ± 0.6	−12.93	40.85			
130006	SPM	32.5 ± 1.6	−12.89	40.81			
130021	SPM	26.4 ± 6.1	−12.88	40.91			
131009	SPM	24.7 ± 3.1	−13.09	40.74			
157032	SPM	1.2 ± 1.5	−14.04	39.70			
157044	SPM	39.8 ± 2.0	−13.17	40.55			
157064	SPM	11.3 ± 6.4	−13.10	40.59			
158036	SPM	11.4 ± 3.4	−12.82	40.89			
158094	SPM	19.1 ± 5.6	−13.19	40.69			
158105	SPM	16.8 ± 2.5	−13.02	40.72			
159008	SPM	23.2 ± 7.1	−12.77	41.04			
159033	SPM	2.1 ± 3.3	−13.82	40.03			
159059	SPM	57.0 ± 9.2	−12.68	41.15			
159061	SPM	4.2 ± 1.7	−13.56	40.20			
159095	SPM	5.0 ± 1.1	−13.53	40.22			
159096	SPM	22.4 ± 4.3	−13.06	40.60			

TABLE 3—*Continued*

		This Work			Literature		
CGCG (1)	Telescope (2)	Hα EW (Å) (3)	Hα Flux (4)	Hα Luminosity (5)	Hα EW (Å) (6)	Hα Flux (7)	Reference (8)
159097	SPM	17.2 ± 3.2	−13.33	40.42			
159101	SPM	61.0 ± 1.4	−12.97	40.79			
159102	SPM	31.1 ± 1.0	−12.59	41.16			
160005	SPM	2.4 ± 2.1	−13.68	40.00			
160007	SPM	−1.4 ± 1.5	...	...			
160018	SPM	−3.0 ± 1.7	...	...			
160020	SPM	35.0 ± 0.8	−12.98	40.49			
160024	SPM	0.4 ± 3.2	−14.67	39.09			
160025	SPM	2.5 ± 1.2	−13.50	40.26			
160026	SPM	33.4 ± 2.5	...	...			
160026	SPM	33.4 ± 2.9	−13.07	40.69			
160032	SPM	10.1 ± 2.4	−13.37	40.39			
160050	SPM	74.5 ± 8.4	...	...			
160055	STW	33.8 ± 1.3	−12.51	41.24	23 ± 4	−12.65	1
160064	SPM	64.8 ± 3.7	−13.12	40.63			
160067	SPM	75.1 ± 13.2	−12.86	40.90			
160073	SPM	23.4 ± 3.7	−13.13	40.62	24 ± 7	−13.15	1
160076	SPM	47.2 ± 6.1	−13.14	40.61	27 ± 7	−13.31	1
160081	SPM	−3.8 ± 0.8	...	...			
160086	SPM	39.3 ± 5.8	−13.22	40.53	58 ± 8	−13.03	1
160088	SPM	15.2 ± 3.0	−12.97	40.78			
160095	SPM	3.9 ± 4.5	−12.99	40.77	7 ± 2	> −12.72	1
160097	SPM	−0.3 ± 0.8	...	...			
160098	SPM	20.4 ± 6.0	−13.15	40.60			
160107	SPM	−4.5 ± 0.6	...	...			
160127	SPM	68.1 ± 16.0	−12.84	40.92			
160128	SPM	79.0 ± 17.6	−12.86	40.90			
160139	SPM	53.4 ± 10.4	−12.73	40.70			
160146	SPM	−4.8 ± 8.0	...	...			
160168	SPM	14.7 ± 10.0	−12.82	41.01			
160192	SPM	2.1 ± 7.1	−13.58	40.15			
160260 S.....	SPM	−3.5 ± 1.6	...	...			
160260	SPM	7.9 ± 2.3	−13.03	40.72	9 ± 2	−12.77	1
161063	SPM	22.2 ± 7.7	−13.20	40.60			
224004	SPM	22.0 ± 5.5	−12.63	40.86			
224004 S.....	SPM	39.5 ± 5.3	−13.22	40.27			
224038	SPM	122.5 ± 2.7	−12.24	41.77			

References.—(1) Kennicutt et al. 1984; (2) Moss et al. 1988.

Column (*1*).—CGCG galaxy name.

Column (*2*).—Telescope used.

Column (*3*).—Total equivalent width from the present work, along with its statistical uncertainty.

Columns (*4*), (*5*).—Logarithm of the integrated flux (ergs cm^{-2} s^{-1}) and luminosity (ergs s^{-1}) from the present work. These two quantities are given only for targets observed under photometric conditions.

Columns (*6*), (*7*).—Equivalent width with error and flux from the literature.

Column (*8*).—References.

Figure 4 shows the comparison between the EW (Fig. 4*a*) and flux (Fig. 4*b*) measurements reported in this paper and those found in the literature for the objects in common. Fluxes and EWs from KK83, KBS84, and GBK91 have been multiplied by 1.16, as suggested by KTC94, in order to account for the continuum flux overestimate due to the inclusion of the telluric absorption band near 6900 Å in the sideband filter.

4.1. *Comments on Individual Objects*

97073.—Figure 3*a* reports the SPM net frame.

97093.—There is a severe disagreement for this galaxy between the present measurement and the value found by Moss et al. (1988) in their objective-prism survey of A1367. There are no apparent reasons to suspect that our data, which were obtained under photometric sky conditions, are bad. Moreover, two early-type galaxies (97088 and 97094) in the frame of 97093 (the redshift of 97094 does not match the on-band filter) result, as expected, in a null net Hα flux. However, a measured $U-B = -0.31$ is consistent with the Moss et al. Hα value.

97129.—Stray light from a nearby bright star contaminates the frame.

98078.—This galaxy, companion to 98081, was classified as elliptical on the PSS because of its featureless appearance. However, it is one of the strongest Hα emitters, with EW ≈ 82 Å. This emission, almost entirely nuclear, is probably caused by the gravitational interaction with its companion and/or with a third, fainter object in the vicinity (clearly seen in the net frame), whose redshift is not presently available.

160050.—At the time of the observation presented in this paper (1995 April), a redshift of 5319 km s^{-1} was available (Tifft & Gregory 1976). Thus we used the 6683 Å filter to obtain the on-band frame and the 6603 Å for the off-band. After reducing the data, we found to our disappointment that more flux and more structure showed up in the off-band frame. However, 1 year later we obtained a spectrum of this galaxy for another project. To our surprise we found

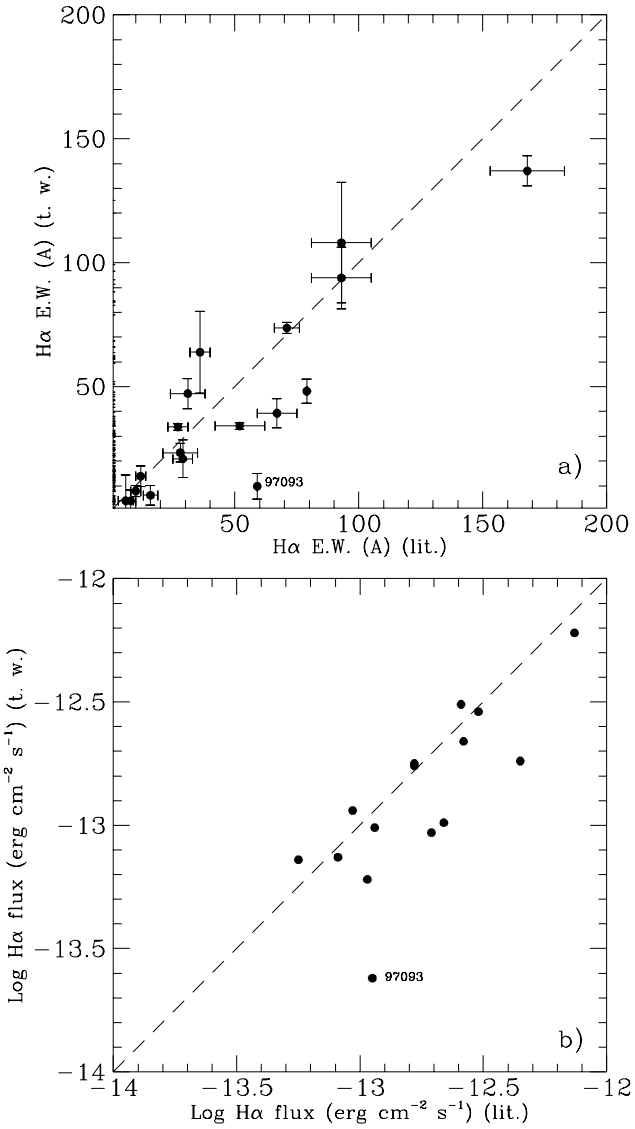

FIG. 4.—Comparison between the (*a*) EW and (*b*) flux measurements from this work and those found in the literature.

that the true redshift is 2496 km s^{-1}. Thus it turns out that our Hα measurement is useful but with reversed filters.

160055.—The off-band frame was contaminated by some stray light from a nearby bright star, which produces a faint diffuse feature at the southeast edge of the galaxy. The net flux from the galaxy might be slightly underestimated accordingly.

224004 S.—No redshift is available for this object, so the filters adopted for 224004 could not match the Hα line. The Hα flux should be considered a lower limit.

224038.—This peculiar object in A2197 might be the remnant of a galaxy collision. The complex velocity field in this galaxy was studied by Maehara et al. (1988).

5. ANALYSIS

To complement our imaging survey, we use in the following analysis Hα data taken from the literature. Table 4 summarizes the data in the Cancer and Virgo Clusters and in the Coma supercluster regions.

Column (*1*).—CGCG designation (Zwicky et al. 1961–1968).

TABLE 4

REFERENCE DATA

CGCG (1)	NGC (2)	UGC (3)	Hα EW (Å) (4)	Reference (5)
14062	4517	7685	15 ± 3	1
14068	4536	7732	18 ± 4	2
14110	4632	7870	34 ± 3	2
42045	4303	7420	34 ± 3	2
42083	4365	7488	2 ± 3	2
42105	4416	7541	20 ± 2	1
42106	4420	7549	40 ± 5	2
42134	4472	7629	−1 ± 2	2
42144	4496	7668	33 ± 5	2
42155	4526	7718	−1 ± 2	2
42159	4535	7727	14 ± 3	2
43041	4713	7985	66 ± 2	1
43071	4808	8054	43 ± 7	2
43093	4900	8116	40 ± 4	2
69088	4178	7215	23 ± 3	2
69092	4189	7235	20 ± 5	2
69110	4212	7275	20 ± 3	2
70024	4294	7407	55 ± 5	2
70025	4299	7414	71 ± 7	2
70058	4374	7494	3 ± 2	2
70067	4390	7519	23 ± 2	1
70072	4406	7532	−1 ± 3	2
70082	4411	7546	24 ± 5	1
70139	4486	7654	1 ± 3	2
70188	4568	7776	14 ± 2	2
70189	4567	7777	14 ± 2	2
70192	4569	7786	6 ± 2	2
70194	4571	7788	10 ± 2	2
70197	4579	7796	4 ± 2	2
71015	4647	7896	16 ± 2	1
71019	4654	7902	30 ± 2	1
71043	4689	7965	13 ± 2	2
71045	4698	7970	6 ± 2	1
71092	4866	8102	−2 ± 3	2
97026	...	6583	88 ± 6	3
97044	...	6625	26	4
97067	...	6670	21	4
97068	...	...	44 ± 5	3
97070	3827	6673	53 ± 3	5
97072	...	...	5 ± 3	3
97091	3840	6702	23 ± 3	3
97120	3860	6718	4 ± 2	3
97121	...	6719	−1 ± 3	3
97122	3859	6721	46 ± 7	3
97149	...	...	13 ± 5	5
98002	...	...	34	4
98041	...	7049	66 ± 11	5
98046	4076	7061	8 ± 7	5
98077	4152	7169	33 ± 8	2
98085	...	...	29 ± 4	5
98130	4237	7315	6 ± 2	2
98144	4254	7345	32 ± 1	2
99023	4293	7405	2 ± 2	2
99024	4298	7412	17 ± 2	1
99030	4321	7450	18 ± 1	2
99045	4382	7508	1 ± 3	2
99076	4501	7675	6 ± 2	2
99096	4548	7753	3 ± 1	2
99098	4561	7768	18 ± 3	2
99106	4595	7826	11 ± 5	2
100004	4651	7901	20 ± 2	2
100005	IC 3725	7923	19 ± 3	5
119016	2545	4287	10 ± 2	3
119027	...	...	13 ± 5	5
119029	...	4308	19 ± 3	3
119040	...	...	12 ± 2	3
119041	...	4324	5 ± 3	3
119043	...	...	24 ± 4	3
119044	...	...	33 ± 8	3
119046	...	4329	27 ± 4	3
119047	...	...	38 ± 4	3

TABLE 4—*Continued*

CGCG (1)	NGC (2)	UGC (3)	Hα EW (Å) (4)	Reference (5)
119050.....	2558	4331	5 ± 2	3
119051.....	...	...	33 ± 11	3
119053.....	...	...	42 ± 4	3
119054.....	IC 2293	...	13 ± 4	5
119057.....	2565	4334	3 ± 1	3
119059.....	...	...	56 ± 14	5
119061.....	...	...	−1 ± 4	3
119062.....	...	4344	17 ± 4	3
119070.....	...	4361	27 ± 8	3
119080 E	IC 2338	4383	52 ± 4	5
119080 W	IC 2339	4383	59 ± 4	5
119083.....	...	4386	11 ± 3	3
119091.....	2582	4391	2 ± 2	3
119092.....	...	4399	28 ± 7	3
119103.....	...	4414	2 ± 3	5
127018.....	...	...	16 ± 5	5
127025 N	3808	...	21 ± 4	5
127025 S	3808	6643	22 ± 4	3
127038.....	3832	6693	16 ± 2	3
127039.....	...	...	48 ± 5	5
127046.....	...	...	61 ± 11	4
127049.....	...	...	59 ± 4	4
127050.....	...	6743	16 ± 5	3
127051 N	IC 732	...	26 ± 5	5
127051 S	...	...	38 ± 3	4
127055.....	...	...	43 ± 6	4
127060.....	3902	6790	42 ± 9	1
127068.....	...	...	26 ± 7	5
127071.....	...	...	52 ± 5	5
127073.....	IC 742	6822	3 ± 3	3
127074.....	...	...	45 ± 4	4
127082.....	...	...	22 ± 3	3
127095.....	3947	6863	15 ± 3	3
127100.....	...	6876	10 ± 3	3
127104.....	...	6887	−1 ± 2	5
127123.....	4018	6966	25 ± 4	5
128003.....	...	...	41 ± 4	5
128016.....	...	...	35 ± 4	5
128023.....	4092	7087	17 ± 3	5
128049.....	...	...	20 ± 4	5
128063.....	...	7270	4 ± 7	5
128080.....	...	...	24 ± 2	5
129012.....	IC 3581	...	28 ± 7	5
129021.....	...	...	24 ± 3	5
129022.....	IC 813	7928	8 ± 3	5
130001.....	4826	8062	4 ± 1	2
130008.....	...	...	49 ± 5	3
130014.....	IC 854	...	20 ± 3	5
130024.....	4215	8336	4 ± 4	5
157012.....	...	...	30 ± 5	5
157035.....	3891	6772	19 ± 2	5
158009.....	...	7064	17 ± 2	5
158010.....	...	...	22 ± 6	5
158038.....	...	...	23 ± 4	5
158054.....	...	...	72 ± 7	5
158055.....	...	7286	−1 ± 5	5
158071.....	4274	7377	4 ± 4	2
158081.....	...	7395	24 ± 4	5
158098.....	IC 3263	...	10 ± 4	5
159031.....	IC 3592	7789	9 ± 5	5
159040.....	...	7818	26 ± 9	5
159076.....	IC 821	7957	15 ± 4	3
159090.....	...	...	22 ± 5	3
159091.....	4735	...	6 ± 4	5
159099.....	...	8013	6 ± 8	3
160011.....	4793	8033	54 ± 2	1
160015.....	...	...	−3 ± 4	5
160036.....	...	...	8 ± 3	5
160058.....	...	...	22 ± 5	3
160096 N	4922	8135	39 ± 10	5
160096 S	4922	8135	7 ± 4	5
160102.....	IC 4088	8140	6 ± 4	3

TABLE 4—*Continued*

CGCG (1)	NGC (2)	UGC (3)	Hα EW (Å) (4)	Reference (5)
160106.....	...	...	20 ± 4	3
160121.....	...	8161	7 ± 7	3
160137.....	4966	8194	11 ± 4	3
160148.....	...	8229	7 ± 4	3
160151.....	...	...	28 ± 8	5
160152 W	5000	8241	17 ± 3	3
160156.....	...	8259	10 ± 4	5
160182.....	...	8359	12 ± 3	5
160212.....	IC 3949	8096	−1 ± 2	3
160257.....	4907	...	6 ± 3	3
161048.....	...	...	3 ± 2	5
161052.....	...	...	48 ± 5	5
161071.....	...	8496	48 ± 7	5
161073.....	...	8498	4 ± 3	5

REFERENCES.—(1) Romanishin 1990; (2) Kennicutt & Kent 1983; (3) Kennicutt et al. 1984; (4) Moss et al. 1988; (5) Gavazzi et al. 1991.

Columns (*2*), (*3*).—NGC/IC and UGC names.

Columns (*4*), (*5*).—Hα equivalent width, along with its error and source reference.

5.1. *Dependence of the SFR on Hubble Type and Mass*

In this section we use the Hα EWs reported in Tables 3 and 4 in order to study the relationship between the current star formation and other photometric properties of disk galaxies. First we show in Figure 5*a* the relation between the Hα EW and morphological type. The Hubble classification is represented by discrete numerical classes: 3 = Sa, 4 = Sab, ..., 7 = Sc, 8 = Irr/Pec. To avoid superposition of points, we added to each class a random number between −0.3 and 0.3. The majority of galaxies in our sample have small angular size (1′–2′), and thus the classification error is probably up to two bins in Hubble type. In particular, because of the adopted classification scheme (see col. [12] of Table 1), the Pec objects might in fact belong to any of the earlier type bins. Nevertheless, despite the uncertainty in our classification, Figure 5*a* shows a definite trend of Hα EW with type. In fact, the average Hα EW among types Sa is 5.3 ± 1.9 Å, significantly lower than 24.5 ± 3.3 Å found among types Sc (see also Roberts & Haynes 1994; KTC94).

To further investigate the reasons for the residual scatter found within each morphological class (see Fig. 5*a*), we analyze the dependence of the Hα EW on the galaxy's mass, a quantity carrying a more direct physical meaning than the Hubble type. Following GPB96, we use the *H*-band luminosity as a tracer of the dynamical mass of disk galaxies (log $M_{\rm dyn} = \log L_H + 0.66$, solar units) to show in Figure 5*b* that the Hα EW decreases significantly with increasing mass. Although the relation appears noisy and nonlinear, low-mass systems ($9 < \log L_H < 10$) show high (40 Å) average EW, weakly decreasing with mass. The order-of-magnitude scatter found in this interval probably reflects the presence or the absence of episodes of star formation of short duration, which is governed primarily by the local gas instability (see Kennicutt 1989). At $\log L_H > 10$, the Hα EW drops to zero, with an even higher scatter than in the low-mass regime. If one divides the data into three bins of decreasing Hα ($0 < \log$ Hα < 1, $1 < \log$ Hα < 1.6, and $\log$ Hα > 1.6), the corresponding average $\log L_H$ is 10.9, 10.4, and 10.0, i.e., an approximately inverse linear proportionality.

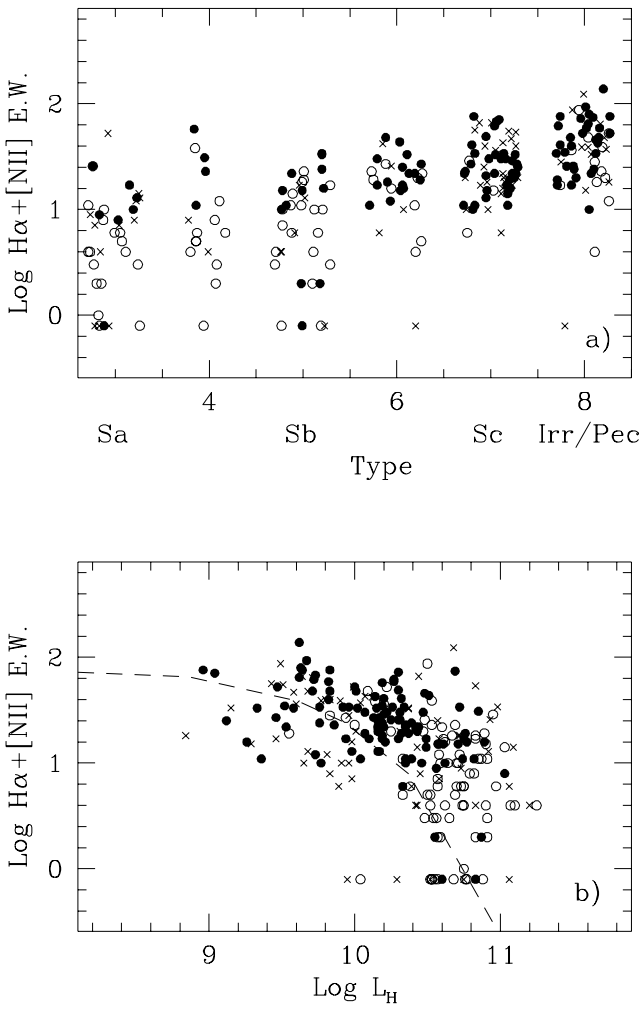

FIG. 5.—Correlation between Hα EW and (*a*) morphological type and (*b*) *H*-band luminosity. Types are given by discrete numerical classes. To avoid overplotting, a random number between −0.3 and 0.3 has been added to each numerical type. Filled circles represent disk galaxies, open circles represent bulge galaxies, and crosses are used for those objects for which no structural information is available. Galaxies with null Hα EW are plotted at log Hα EW = −0.1. The dashed line shows the model adapted from KTC94 to contain the inverse dependence of τ on mass, as discussed in § 6.

5.2. *Dependence of the SFR on Bulge-to-Disk Ratio*

One of the most clear-cut results of GPB96 is that the presence in the near-infrared of centrally peaked structures (bulges/nuclei) strongly correlates with the total *H* (1.65 μm) luminosity or mass (see their Fig. 9). These authors used the model-independent parameter C_{31}, defined as the ratio of the radii containing respectively 75% and 25% of the total *H*-band light, and found C_{31} in the range 1–3 for pure disk objects, and $C_{31} > 3$ in galaxies with prominent bulges.

Given this result, it is important to investigate whether the inverse correlation between SFR and mass, reported in the previous section, follows from the anticorrelation between Hα EW and C_{31}—in other words, whether the Hα EW is strong in pure disk galaxies and weak in bulge-dominated galaxies, as claimed by Devereux & Young (1991). However, KTC94 showed that variations of Hα EW do not simply reflect different contributions of bulge light to the continuum, but real variations of the disk SFR. Points in Figure 5 (and in the following figures, unless otherwise specified) are coded according to C_{31}: filled circles are pure disks, open circles are bulge-dominated systems, and crosses indicate those objects for which no structural information is available. Pure disks dominate the low-L_H/high-Hα/late-type regime. Also, in Figures 6*a*–6*c*, where we plot the Hα-L_H relation in separate morphological type bins, the segregation according to C_{31} is apparent, and enhanced in Figures 6*d* and 6*e*.

It is evident that the quantities C_{31}, Hα, L_H, and morphological type are not independent of one another, as illustrated in Figure 7. However, while both Hα (Fig. 7*a*, extracted from Fig. 5*b*) and C_{31} (Fig. 7*b*) are strongly related with L_H, the correlation of Hα with C_{31} (Fig. 7*c*) is poorer: most disk galaxies ($C_{31} < 3$) have high SFRs, but a significant fraction of them have log Hα < 1. Any value of Hα EW may be found among bulge-dominated objects.

In conclusion, we claim that the dependence of Hα EW on mass (*H* luminosity) is not entirely induced by the dependence of the bulge-to-disk ratio on luminosity. The primary dependences are those of C_{31} and of Hα EW on mass, and that of Hα EW on C_{31} follows as a consequence.

The secondary, marginal correlation between Hα and C_{31} implies, however, that in bulge-dominated systems the Hα EW might not provide a reliable estimate of the disk SFR, as argued by Devereux & Young (1991). Since by definition the EW is computed from the Hα net flux normalized to the red continuum, it would be artificially reduced by a strong contribution of the bulge to the continuum. To assess this important point, we investigate the correlation between the Hα EW and another SFR indicator, namely, the Hα surface brightness ($\Sigma_{H\alpha}$). The latter parameter is defined as the ratio of the Hα net line flux to the disk area (computed using a_{25}, the diameter measured in the *B* band at the 25 mag arcsec^{-2} isophote). The normalizing area is independent of the bulge properties, and thus $\Sigma_{H\alpha}$ should yield a reliable estimate of the disk SFR. In Figure 8, we plot (adopting the usual symbols coded according to the bulge-to-disk ratio) the two SFR parameters against each other (Fig. 8*a*); the two quantities are linearly correlated, and disks and bulges are nicely segregated along the diagonal line. Furthermore, we show in Figure 8*b* that the correlation between $\Sigma_{H\alpha}$ and L_H is qualitatively similar to that found between Hα EW and L_H (Fig. 5*b*).

We conclude that Hα EW is marginally affected by the bulge contribution and thus can be used as a reliable estimate of the integrated SFR. Moreover, another advantage of using Hα EW over $\Sigma_{H\alpha}$ is that the accuracy of the former is about 10%, while the uncertainty on the area determination, up to 100%, reflects into a similar uncertainty on $\Sigma_{H\alpha}$.

5.3. *Frequency Distribution of the* Hα *EW*

The analysis carried out in the previous section has shown that the SFR in disk galaxies is anticorrelated with their luminosity (mass). This finding makes the determination of the characteristic SFR properties of galaxies meaningless unless a luminosity range is specified, i.e., if samples selected according to well-defined completeness criteria are used. The Hα survey presented in this paper contains in fact a subsample complete to $M_p = -18.8$, being selected from a magnitude-limited subsample complete down to $m_p = 15.4$, entirely composed of objects lying at a constant distance (70 Mpc, containing both isolated and cluster members). With these data we construct the frequency distribution of the Hα EW in bins of log EW = 0.4, as shown

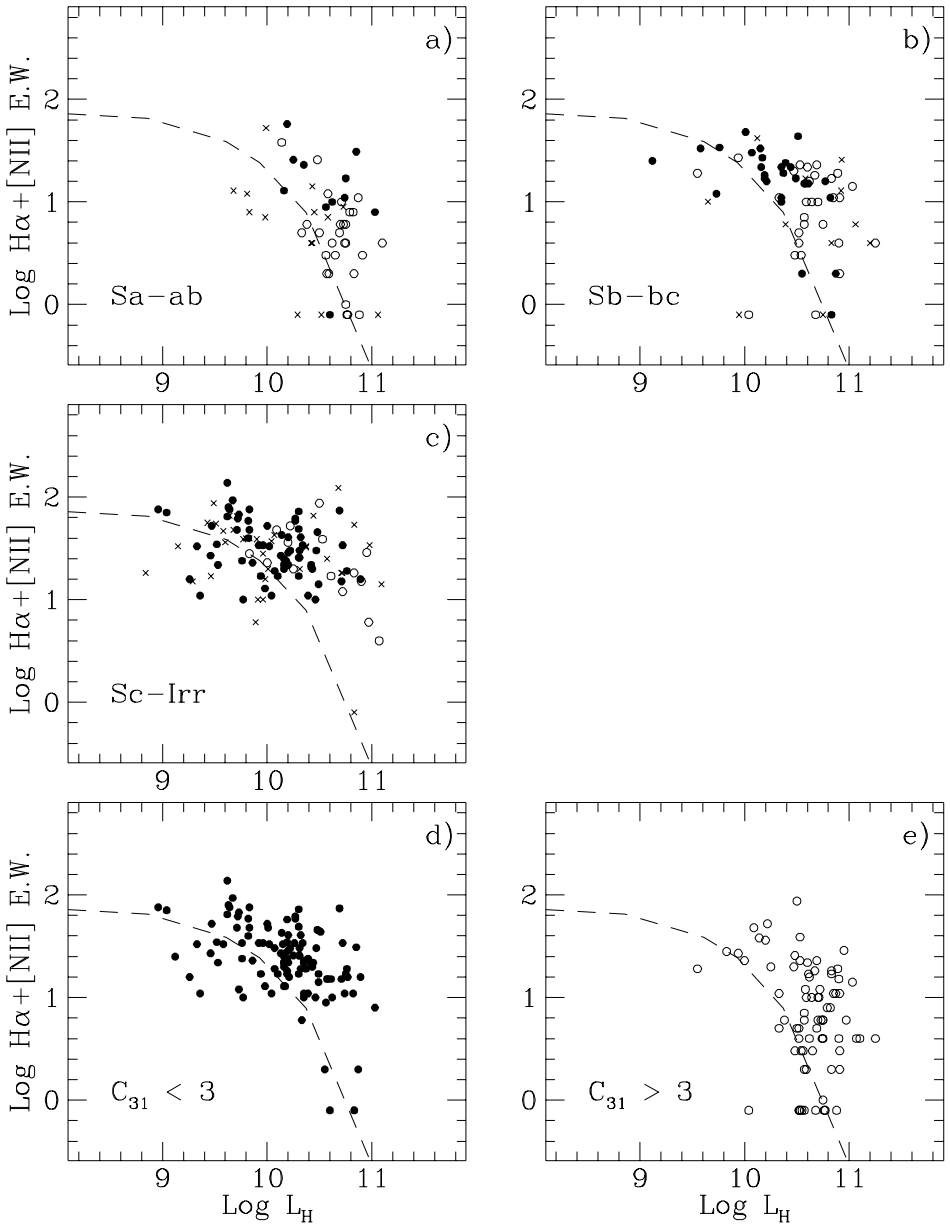

FIG. 6.—(*a–c*) Correlation between Hα EW and *H*-band luminosity in bins of Hubble type. The same correlation is given separately for (*d*) disk and (*e*) bulge galaxies. Symbols are the same as in Fig. 5.

in Figure 9*a*. It appears that, for galaxies brighter than $M_p = -18.8$, the average Hα EW is 22 ± 2 Å. This value would increase if an intrinsically fainter sample was selected. The distribution peaks at EW = 25 Å. Over 40% of galaxies have their EW in the range 16–40 Å. Fewer than 15% of galaxies have null EW: these are either S0/S0a galaxies misclassified as spirals or high-mass systems.

5.4. *Environmental Dependence of SFR*

Given the conclusions of the previous sections, it also follows that the comparison between the SFR properties of galaxies found in and outside clusters is meaningful only for samples with equal limiting optical luminosity. The frequency distributions for two different samples, one consisting of 40 cluster members, the other of 66 isolated galaxies, both with a limiting magnitude $m_p = 15.4$, are compared in Figures 9*b* and 9*c*. In Figure 9*b* the membership is according to the criterion of column (10) of Table 1 ("caustics"), while in Figure 9*c* the membership is according to the criterion of column (9) (angular separation). As can be seen from these figures, the distributions are insensitive to the adopted membership criterion. Moreover, no significant difference is found between the cluster distribution and that for the isolated galaxies, as derived using the Kolmogorov-Smirnov test (the probability that the cluster and isolated distributions derive from the same parent population is 2.5%). This indicates, contrary to common belief, that cluster spiral + Irr galaxies have mean SFR values indistinguishable from those of the isolated objects. The histograms in Figures 9*b* and 9*c* suggest, however, that the cluster sample has a less pronounced peak at log Hα EW = 1.4 than the isolated one. Conversely, there is marginal evidence for an overabundance of intermediate Hα EW (0–10 Å) among cluster objects. However, based on the data in

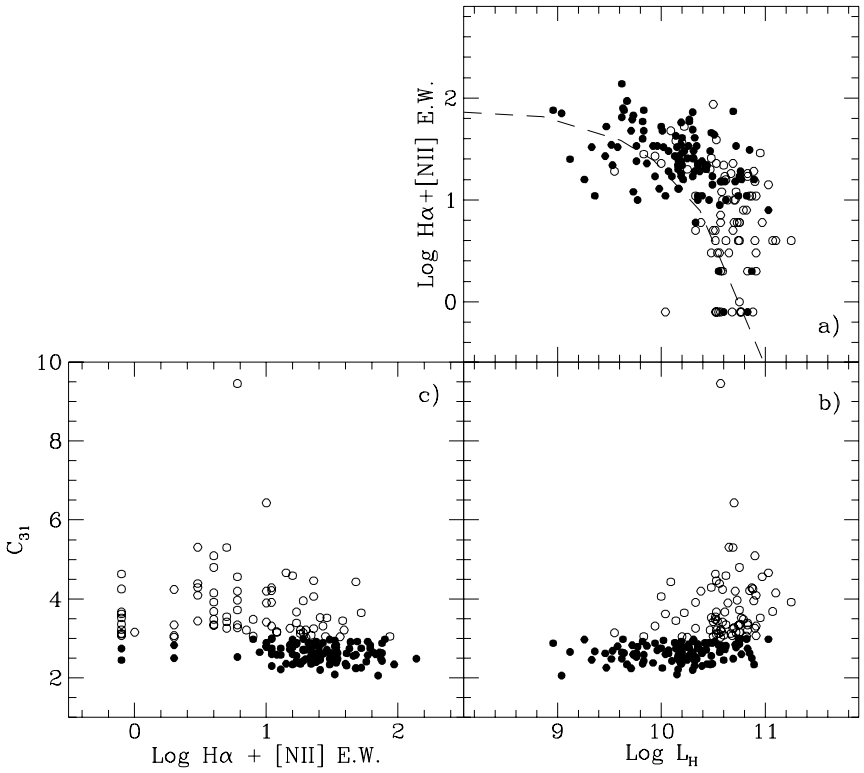

FIG. 7.—Mutual relations between Hα EW, L_H, and C_{31}. Symbols are the same as in Fig. 5.

our possession, these differences are not statistically significant.

It is well known that late-type galaxies avoid the central regions of rich clusters. This is clearly the case in the Coma Cluster (see Andreon 1996) and, to a lesser extent, in A1367. It has been claimed that spirals at the periphery of the Coma Cluster have bluer than average color indexes. Donas, Milliard, & Laget (1995), for example, found an enhancement of objects with blue UV$-B$ excess. If this reflects an enhanced SFR, it is expected that a similar pattern should show up in our data. The radial distributions of the Hα EW are given up to 7° projected separation from Coma and A1367 in Figures 10*a* and 10*b*, respectively. Points are coded according to L_H to stress once more the inverse proportionality between SFR and mass. Except for a marginal increase of the dispersion near the center of A1367, the only apparent pattern is a relatively large fraction of faint (log $L_H \leq 10.0$) galaxies with large Hα EW in the shell contained between 1° and 2° of projected radii around Coma. However, we suggest that this effect is due to a mass segregation instead of a real enhancement of the SFR. In fact, if we remove, to first order, the luminosity (mass) dependence, by multiplying Hα EW by the corresponding L_H (as derived in three intervals in § 5.1), any

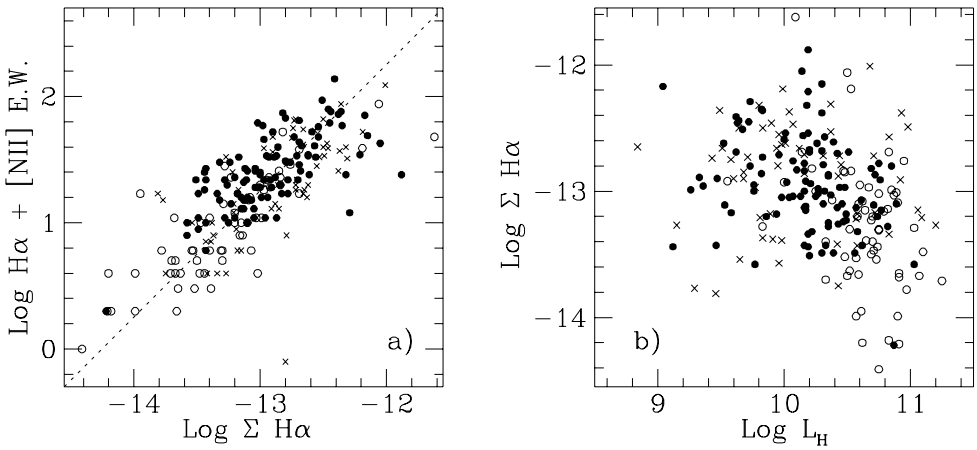

FIG. 8.—Correlation (*a*) between Hα EW and $\Sigma_{H\alpha}$ (in ergs cm^{-2} s^{-1} arcmin^{-2}) and (*b*) between $\Sigma_{H\alpha}$ and L_H. Symbols are the same as in Fig. 5. The straight line in (*a*) has a slope of 1.

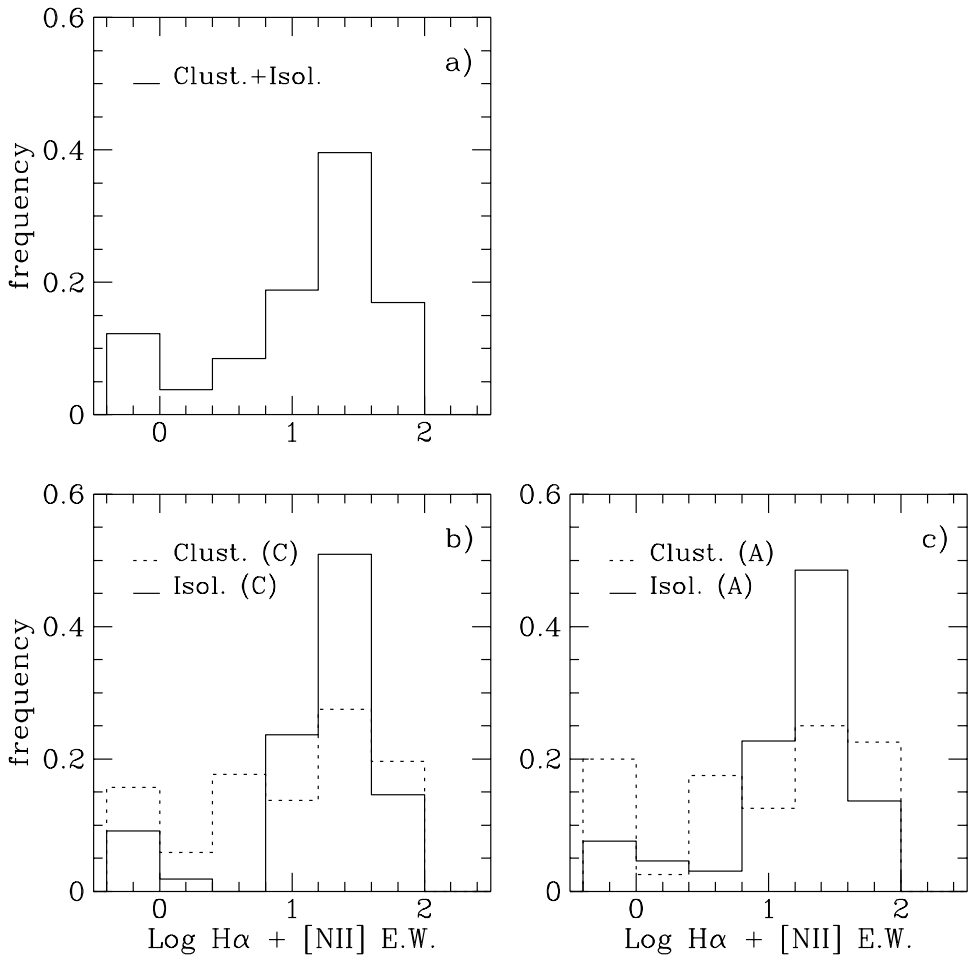

FIG. 9.—(*a*) Frequency distribution of the Hα EWs for the complete sample of isolated and cluster galaxies with $M_p \leq -18.8$. Isolated galaxies (*solid line*) and cluster members according to the criteria given in cols. (9) (angular separation) and (10) (caustics) of Table 1 (*dotted line*) are shown in (*c*) and (*b*), respectively.

evidence for radial gradients is canceled (see Figs. 10*c* and 10*d*).

6. DISCUSSION AND CONCLUSIONS

The main results of the present work can be summarized as follows:

1. The present SFR properties of spiral galaxies, as derived from a representative sample of the local universe, increase with increasing Hubble type.

2. These properties do not show a significant dependence on the explored range of local galaxy density, spanning 1 order of magnitude between isolated supercluster objects and members of Coma-like clusters.

3. The present SFR shows a definite negative trend with *H*-band luminosity. The average Hα EW increases from 0 to about 30 Å with decreasing log L_H from 11 to 9, i.e., with decreasing dynamical mass from log $M = 11.5$ to 9.5 (solar units). This statement holds strictly for disk galaxies included in the present analysis. Nothing can be concluded about the mass dependence in E + S0's. Hα EW depends also marginally on the bulge-to-disk ratio, but this comes as a consequence of a primary dependence of the bulge-to-disk ratio on L_H.

Point 2 does not mean that the environment is playing no role in the formation and evolution of galaxies. The existence of a strong morphology-density relation, i.e., the environmental dependence of the fraction of early- to late-type galaxies, is not in question. The conclusion of the present work is that galaxies that retain a spiral-Irr morphology at the present cosmological epoch have star formation properties that do not differ in and outside rich clusters. Our observations do not rule out the possibility that galaxies in clusters form primarily as E + S0's and that spiral galaxies have only recently entered the dense cluster environment, falling inward. If $T_{\rm res}$ is the time since their infall, $\tau_{\rm dep}$ is the H I depletion timescale for ram pressure (estimated at a few times 10^8 yr by Gavazzi 1989), and $\tau_{\rm H\,I-H_2}$ is the timescale of the transformation from the atomic to the molecular phase, then we can only conclude that $\tau_{\rm H\,I-H_2} \gg 10^8$ yr, i.e., that these systems are still "burning" the molecular gas that was formed before they entered the cluster environment. This is consistent with the evidence that the molecular gas content of H I–deficient galaxies in rich clusters is normal (see, e.g., Boselli et al. 1997). It cannot be excluded, however, that on a timescale longer than $\tau_{\rm H\,I-H_2}$ these galaxies will run out of gas to fuel a substantial star formation rate and, hence, progressively evolve into anemic systems.

Point 3 has deep implications for models of galaxy evolution, following the line traced by GPB96 and GS96 and the seminal work of Sandage (1986). GPB96 and GS96 argued that the correlation found between the $B-V$, $U-B$, $B-H$, and $UV-V$ color indexes, other Population I indicators,

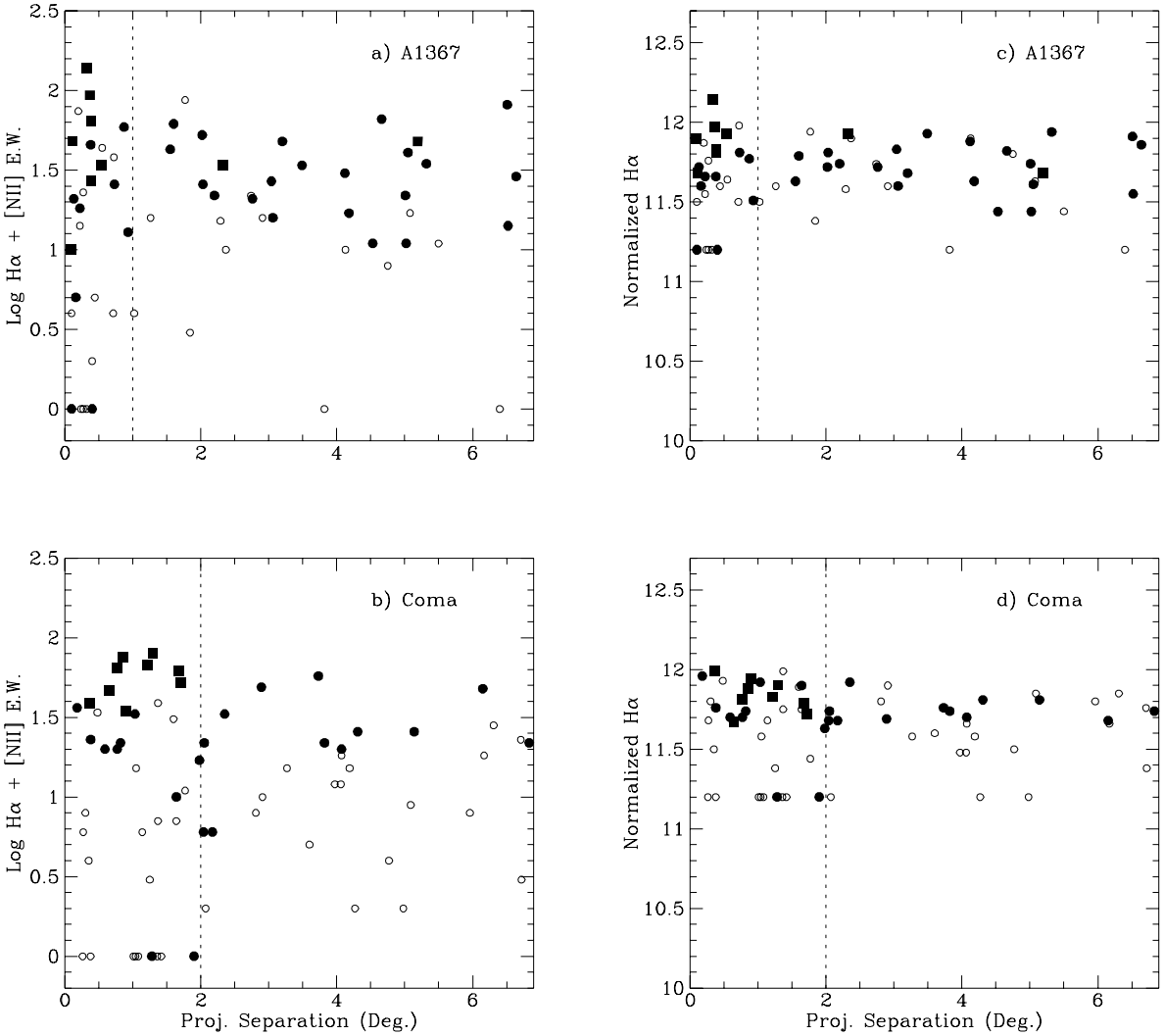

FIG. 10.—Distributions of Hα EW in the (*a*) A1367 and (*b*) Coma Clusters as a function of projected angular separation from the X-ray centroids (in degrees). The vertical lines mark the approximate extent of the Abell clusters (cf. Fig. 1). (*c*, *d*) Projected radial distributions of the "normalized" Hα EW. This parameter helps in removing the inverse dependence between the Hα EW and the *H*-band luminosity (see § 5.1). Squares mark galaxies with $L_H < 10.0$; filled circles mark objects with $10.0 < L_H < 10.5$; empty circles mark galaxies with $L_H > 10.5$.

and the galaxy mass follows from a basic dependence of galaxy evolution on the mass of their progenitor protogalaxies. Adopting a closed-box model (galaxies evolve out of the primeval gas, with some contribution from recycled gas), these authors claim that the presently observed color indexes are consistent with the idea that galaxies are coeval systems (consistent with an age of 6.5–10 Gyr), and that the time dependence of their initial collapse (SFR) follows an exponential relation with the time constant τ inversely proportional to their mass, as $\tau \propto M^{-3.1}$. Massive disk galaxies ($M = 10^{12.5}\ M_\odot$) have a time constant as short as 5×10^8 yr, while low-mass systems ($M = 10^{8.5}\ M_\odot$) are consistent with a star formation history of 10^{10} yr duration.

Adapting the model of GS96 to an age of 10 Gyr (consistent with KTC94), the dependence $\tau \propto M^{-\alpha}$ of τ on mass requires $\alpha = 2.5$. Combining this key argument with the model of KTC94, which predicts the present SFR as a function of τ, we can derive the SFR as a function of mass, as represented by the dashed lines in Figures 5*b*, 6, and 7*a*. We use the model of KTC94 restricted to the case of an exponentially declining SFR with time (case $b \leq 1$), assuming a Salpeter initial mass function (IMF) and solar metallicity (see their Table 1). The model Hα EWs are multiplied by 1.5 to account for the fact that the observed ones contain an equal contribution from the satellite [N II] lines (Kennicutt 1992). The model prediction and the data are in good agreement. The SFR predicted by the model, instead, would fall short with respect to the observed values by a factor of 2 if a Scalo instead of a Salpeter IMF were assumed, or if an extinction correction of about 1 mag, as discussed by KTC94, was applied.

Altogether, we claim that the observed Hα values are found in satisfactory agreement with those predicted by using the simple (perhaps simplistic) assumption that the timescale of a single episode of star formation depends on the system mass as $\tau \propto M^{-2.5}$, without invoking recent bursts of star formation (case $b > 1$). In other words, the best known Population I indicator, namely, the present massive SFR, is predicted by means of a simple evolutionary model in which the mass is the principal parameter governing the collapse timescale of protogalaxies. Massive galaxies had a short, intense burst of star formation shortly after their collapse, thus retaining little gas to fuel the present star formation. Low-mass systems underwent a

much longer, less spectacular episode of star formation, which is still transforming a significant fraction of gas into stars at the present cosmological epoch. We emphasize that the above argument applies strictly to disk (spiral) galaxies.

Our evolutionary scenario has been confirmed by observations of faint galaxies at high redshift. Quoting Cowie et al. (1996): "The more massive forming galaxies seen at $z = 1$–3 are identified as earlier type spirals, whose star formation rates are initially high and then decline rapidly at $z < 1$, while for later type spirals and smaller mass irregulars the star formation rates at $z < 1$ are lower, and the formation process persists to redshifts much closer to the present epoch." Together with GS96, we stress that from the present observations there is no compelling evidence that galaxies are not coeval systems, i.e., the epoch of their formation is a function of their mass, but that the duration of their collapse is inversely proportional to their mass.

We wish to thank R. Kennicutt for providing us with data taken with the Steward 2.3 m telescope, and I. Randone, who contributed to the data reduction. We are grateful to the time allocation committee of the San Pedro Mártir Observatory for the generous allocation. We warmly thank the telescope operators of the San Pedro Mártir Observatory. We are grateful to an unknown referee, whose comments helped to improve the present work. This work was partially supported by CONACYT research grant 211290-5-1430PE (L. C.) and by CARIPLO (G. G.).

REFERENCES

Andreon, S. 1996, A&A, 314, 763
Arimoto, N., & Kodama, T. 1997, in Galaxy Scaling Relations, ed. L. A. N. da Costa & A. Renzini (Berlin: Springer), 132
Boselli A., Gavazzi, G., Lequeux, J., Buat, V., Casoli, F., Dickey, J., & Donas, J. 1997, A&A, 327, 522
Bothun, G. D., & Dressler, A. 1986, ApJ, 301, 57
Bothun, G. D., Romanishin, W., Strom, S. E., & Strom, K. M. 1984, AJ, 89, 1300
Cowie, L. L., Hu, E. M., Songaila, A., & Egami, E. 1996a, ApJ, 481, L9
Devereux, N. A., & Young, J. S. 1991, ApJ, 371, 515
Donas, J., Milliard, B., & Laget, M. 1995, A&A, 303, 661
Gavazzi, G. 1989, ApJ, 342, 718
Gavazzi, G., & Boselli, A. 1996, Astrophys. Lett. Commun., 35, 1
Gavazzi, G., Boselli, A., & Kennicutt, R. 1991, AJ, 101, 1207 (GBK91)
Gavazzi, G., Contursi, A., Carrasco, L., Boselli, A., Kennicutt, R., Scodeggio, M., & Jaffe, W. 1995a, A&A, 304, 325
Gavazzi, G., Pierini, D., & Boselli, A. 1996, A&A, 312, 397 (GPB96)
Gavazzi, G., Randone, I., & Branchini, E. 1995b, ApJ, 438, 590
Gavazzi, G., & Scodeggio, M. 1996, A&A, 312, L29 (GS96)
Kennicutt, R. C., Jr. 1983a, ApJ, 272, 54
———. 1983b, AJ, 88, 483
Kennicutt, R. C., Jr. 1989, ApJ, 344, 685
———. 1990, in The Interstellar Medium in Galaxies, ed. H. A. Thronson & J. M. Shull (Dordrecht: Kluwer), 405
———. 1992, ApJ, 388, 310
Kennicutt, R. C., Jr., Bothun, G. D., & Schommer, R. A. 1984, AJ, 89, 1279 (KBS84)
Kennicutt, R. C., Jr., & Kent, S. M. 1983, AJ, 88, 1094 (KK83)
Kennicutt, R. C., Jr., Tamblyn, P., & Congdon, C. E. 1994, ApJ, 435, 22 (KTC94)
Maehara, H., Hamabe, M., Bottinelli, L., Gouguenheim, L., Heidmann, J., & Takase, B. 1988, PASJ, 40, 47
Moss, C., Whittle, M., & Irwin, M. J. 1988, MNRAS, 232, 381 (MWI88)
Nilson, P. 1973, Uppsala General Catalogue of Galaxies (Uppsala: Uppsala Astron. Obs.)
Roberts, M. S., & Haynes, M. P. 1994, ARA&A, 32, 115
Romanishin, W. 1990, AJ, 100, 373
Sandage, A. 1986, A&A, 161, 89
Tifft, W. G., & Gregory, S. A. 1976, ApJ, 205, 696
Visvanathan, N. 1981, A&A, 100, L20
Zwicky, F., Herzog, E., Karpowicz, M., Kowal, C., & Wild, P. 1961–1968, Catalogue of Galaxies and of Clusters of Galaxies (Pasadena: Caltech)